Characterization of an exhumed high-temperature hydrothermal system and its application for deep geothermal exploration: An example from Terre-de-Haut Island (Guadeloupe archipelago, Lesser Antilles volcanic arc)

Alexiane Favier, Jean-Marc Lardeaux, M. Corsini, Chrystèle Verati, V. Navelot, Y. Géraud, M. Diraison, S. Ventalon, E. Voitus

Characterization of an exhumed high-temperature hydrothermal system and its application for deep geothermal exploration: an example from Terre-de-Haut Island (Guadeloupe archipelago, Lesser Antilles volcanic arc)

A. Favier[a-b-c*], J-M. Lardeaux[b-d], M. Corsini[b], C. Verati[b], V. Navelot[c], Y. Géraud[c], M. Diraison[c], S. Ventalon[e] and E. Voitus[f]

a: Université des Antilles-CNRS-Université de Montpellier-Géosciences Montpellier, Campus de Fouillole, 97159 Pointe à Pitre Cedex, Guadeloupe, France
b: Université Côte d'Azur-Observatoire de la Côte d'Azur-CNRS-IRD-Géoazur, 250, rue Albert Einstein, Sophia Antipolis, 06560 Valbonne, France
c: Université de Lorraine-CNRS-GeoRessources, F-54000, France
d: Czech Geological Survey, Centre for Lithospheric Research, Klárov 3, 118 21 Prague 1, Czech Republic
e: UMR 8187 Laboratoire d'Océanologie et de Géosciences, Université de Lille, Avenue Paul Langevin, 59655 Villeneuve d'Ascq, France
f: Université des Antilles, ESPE, Morne Ferret, BP 517, 97178 Abymes cedex, France

* Corresponding author (alexiane.favier@univ-lorraine.fr; permanent address: alexianefavier@outlook.com)

Abstract

We present integrated structural, petrological, mineralogical and geochemical investigations conducted on an exhumed hydrothermal system identified in Terre-de-Haut Island (Guadeloupe archipelago). This work demonstrates, for the first time, the occurrence of ductile shear zones, marked by the development of spaced schistosity planes generated by pressure-solution processes. We unravel first that the development of spaced schistosity is coeval with high-temperature hydrothermalism (approximately 350°C) and second that this hydrothermal alteration occurred at a depth of less than 2 kilometres. We highlight, at shallow crustal depths, the record of both vertical and lateral fluid pathways in the studied volcanic arc. Finally, combining this new dataset with the large number of published surface data obtained in the active geothermal system of Bouillante, we propose a conceptual scheme for the studied fossil reservoir to document the roots of magmatic arc-related active geothermal systems and to introduce new perspectives for deep geothermal exploration.

Keywords: exhumed hydrothermal system; hydrothermal fluids pathways; high temperature geothermal reservoir; geothermal exploration; Lesser Antilles arc.

1- Introduction

For many geothermal systems, a significant amount of geological and geophysical surface data is currently available to characterize geothermal resources (Ledru and Guillou-Frottier, 2010; Moeck, 2014). However, deciphering the geological properties of the lowermost part of geothermal reservoirs, i.e., below commonly drilled depths (1.5 kilometres in the case of the Lesser Antilles arc), is, still challenging due to the high economic cost of exploratory drillings and poor knowledge of the mechanical properties of hydrothermalized materials at high P-T conditions (i.e. T > 300°C and P > 2 Kbar). As frequently implemented in the study of oil resources, an effective alternative to address this type of issue is the study of exhumed analogues (e.g., Bouma, 1962; Middleton and Bouma, 1973; Beck and Lehner, 1974; Joseph and Lomas, 2004). This approach was successfully applied to epithermal systems coeval with magmatic activities, which are regarded as fossil geothermal systems (Bouchot and Genter, 2009; Liotta et al., 2010; Cooke D. R. and Simmons S. F. 2000; Garden et al., 2020).

On the west coast of Guadeloupe (Lesser Antilles magmatic arc), a high-energy geothermal system favourable for electricity production was identified in the 1970s in Bouillante Bay (Cormy et al. 1970; Demians d'Archimbaud and Munier-Jolain 1976; Demians d'Archimbaud and Surcin 1976). This geothermal field has been well characterized through geological, geochemical and geophysical investigations and several exploration and production wells (Iundt and Ouzounian, 1984; Abou Akar et al., 1992; Sanjuan and Brach, 1997; Guillou-Frottier, 2003; Lachassagne et al., 2009; Bouchot et al., 2010; Thinon et al., 2010; Calcagno et al., 2012; Gailler et al., 2013). However, despite these efforts, the pathways for fluid and heat transfer in the deepest part of this reservoir are still under debate (Navelot et al., 2018). A hydrothermal system considered a possible exhumed analogue of such a geothermal

reservoir has been identified in the Guadeloupe archipelago, precisely in Les Saintes Islands (Jacques and Maury, 1988; Verati et al., 2016). According to these authors, superposed fault networks structurally control the development of hydrothermal alteration zones, and in a previous paper, we investigated the role of faults, fractures and lithological discontinuities on fluid transfers, hydrothermal alterations and petrophysical properties of volcanic rocks in this area (Navelot et al., 2018). However, in the western arc of the Guadeloupe volcanic archipelago, ductile tectonic structures were recently discovered (Verati et al., 2018; Favier et al., 2019). As demonstrated by numerous authors, the tectonic and kinematic framework, and therefore the regional stress field, has remained unchanged since 5 Ma in this volcanic archipelago (Bouysse and Garrabé, 1984; Julien and Bonneton, 1989; Feuillet et al., 2002, 2004; Mathieu et al., 2011; Corsini et al., 2011; Lardeaux et al., 2013; Münch et al., 2013; Leclerc et al., 2016). Consequently, the goal of this paper is to investigate the relationships between the mineralogical evolution of hydrothermalized rocks and ductile tectonic structures, in Les Saintes Islands, in order to document the roots of active geothermal systems developed in magmatic arcs and to develop new perspectives for deep geothermal exploration.

2- Regional setting

2-1- The Guadeloupe archipelago in the Lesser Antilles arc

The 850 km-long curved Lesser Antilles arc is located at the convergent boundary between the Caribbean and American plates (Figure 1-A; Hawkesworth and Powell, 1980; Bouysse and Westercamp, 1988; Demets et al., 2000). This is the consequence of southwest-directed subduction of the American plates beneath the Caribbean plate with a velocity of approximately 2 cm/yr (Lopez et al., 2006). The crustal thickness of the upper plate supporting the volcanic arc was defined by geophysical investigations at approximately 28 km (Kopp et al., 2011; Gailler et al., 2013). The conductive geothermal gradient of the Lesser

Antilles arc is now well established (Manga et al., 2012) and was measured around the Guadeloupe archipelago in a range between 69.3 ± 1.5 and 98.2 ± 8.8 °C/km (Figure 1-A).

The northern part of the magmatic arc, including the Guadeloupe archipelago (Fig. 1-A), is divided into two subparallel ridges (Westercamp, 1979). The eastern arc is an ancient arc formed by late Oligocene to Pleistocene carbonate platforms (Grande-Terre), while the western arc is composed of a recent chain of volcanic islands (Basse-Terre and Les Saintes) active since 5 Ma (Bouysse and Westercamp, 1990). Basse-Terre Island consists of a cluster of volcanic complexes, frequently called “volcanic chains” (Figure 1-B). From north to south, Samper et al. (2007) recognized the following: the oldest, the Basal Complex, characterized by 4.28 to 2.67 Ma aged volcanism (Favier et al., 2019); the Septentrional Chain, formed between 1.81 and 1.16 Ma; the Axial Chain, active from 1.02 to 0.41 Ma; the Grande Découverte – Trois Rivières Complex (0.20 Ma-recent), including the present-day active La Soufrière volcano (Boudon et al., 1987, 2008); and the Monts Caraïbes Chain built at approximately 0.55-0.47 Ma (Blanc, 1983; Ricci et al., 2017). Southeast of Basse-Terre Island, the Les Saintes archipelago is composed of two islands: Terre-de-Haut Island with 3.63 to 2.00 Ma aged volcanism and Terre-de-Bas Island younger than 1.00 Ma (Jacques et al., 1984; Jacques and Maury, 1988; Zami et al., 2014).

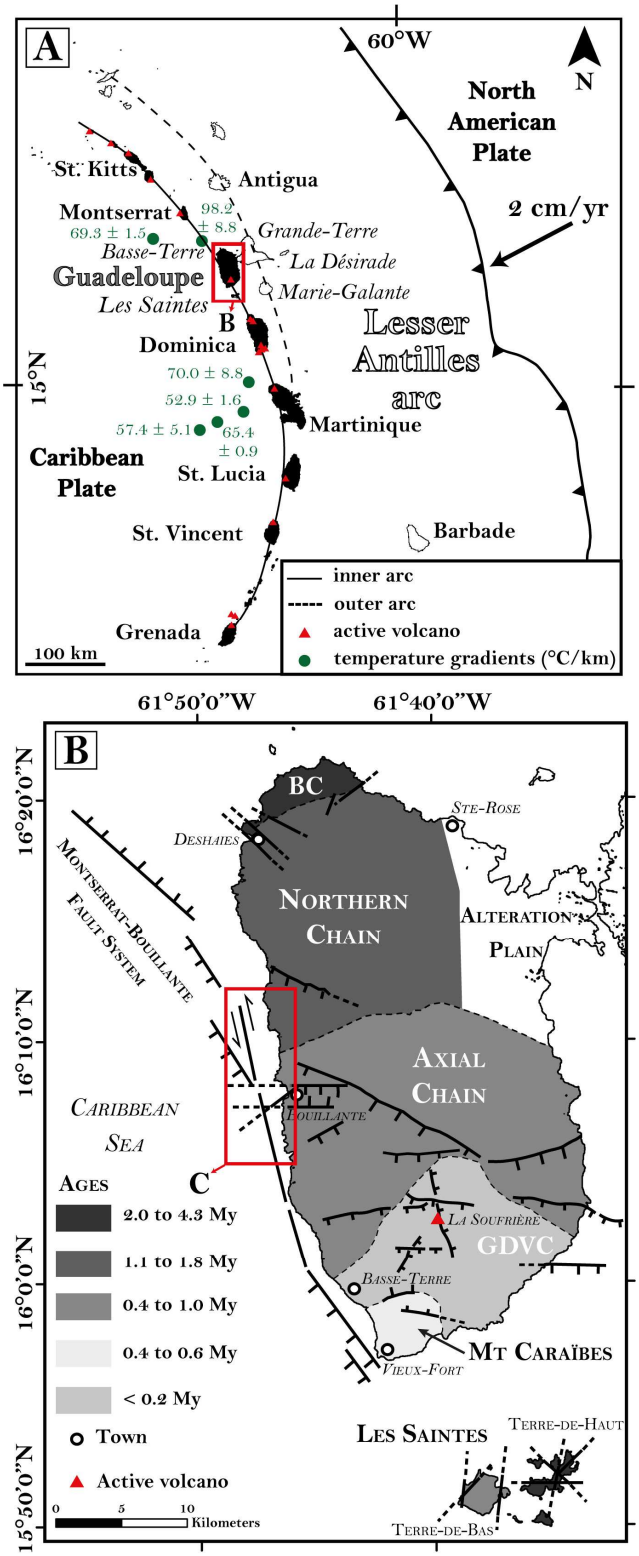

Figure 1: A) Geodynamic setting of the Lesser Antilles arc (after Feuillet et al., 2001; heat flow measurements from Manga et al., 2012), B) Map of the active volcanic arc in Guadeloupe archipelago (i.e. Basse-Terre and Les Saintes) displaying the different volcanic complexes and the main tectonic structures (modified after Boudon et al., 1987; Calcagno et al., 2015; Ricci et al., 2017; Verati et al., 2018 and Favier et al., 2019), BC = Basal Complex; GDVC = Grande Decouverte Volcanic Complex. **(COLOR FOR ONLINE VERSION ONLY / IMAGE SIZE: COLUMN WIDTH)**

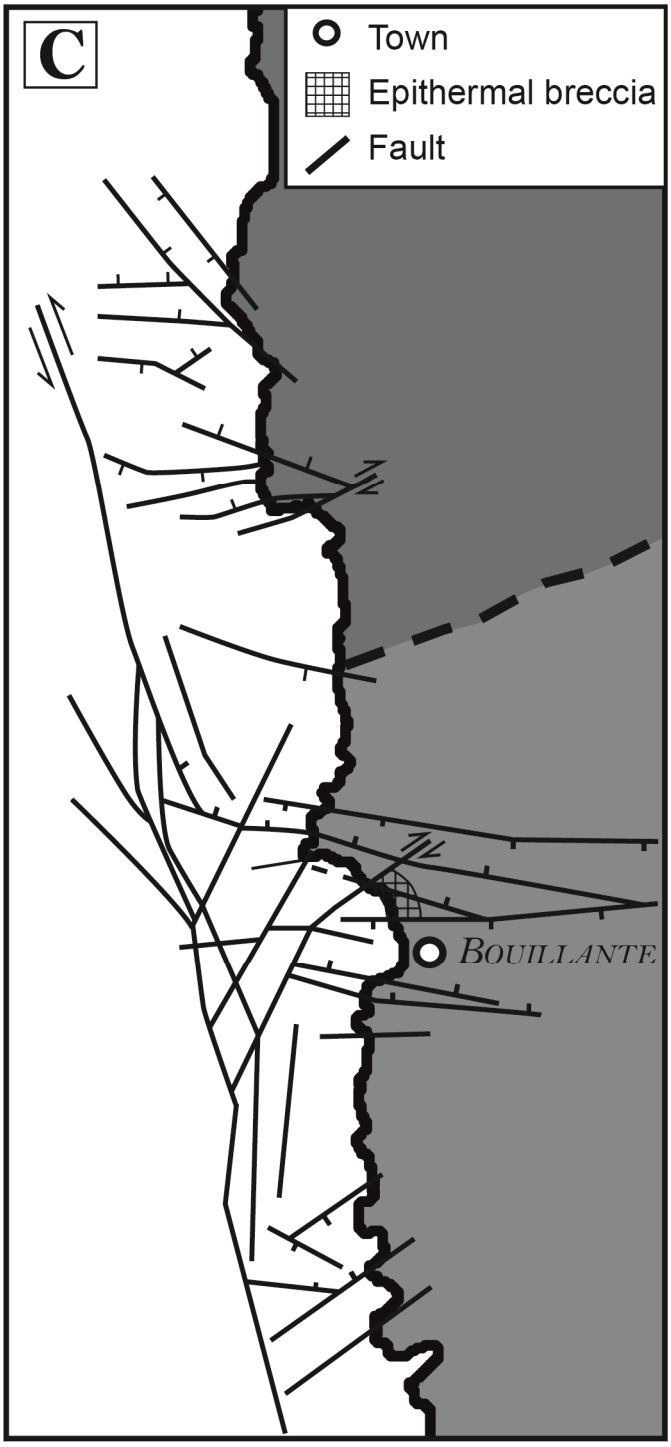

Figure 1: C) Tectonic sketch map of Bouillante area in Basse-Terre Island (modified after Calcagno et al., 2012; Calcagno et al., 2015; Navelot et al., 2018). **(COLOR FOR ONLINE VERSION ONLY / IMAGE SIZE: COLUMN WIDTH)**

2-2- Brittle tectonic framework in the Guadeloupe archipelago:

Regionally, four major brittle fault directions have been identified: N50-N70, N90-N110, N120-N140 and N160-N10. Onshore and offshore investigations (Feuillet et al., 2002, 2004,

2010, 2011; Thinon et al., 2010; Mathieu et al., 2011; Corsini et al., 2011; Laigle et al., 2013; Lardeaux et al., 2013; Münch et al., 2013; De Min et al., 2015; Leclerc et al., 2016; Legendre, 2018; Navelot et al., 2018; Leclerc and Feuillet, 2019) allow the reconstruction of the deformation history on the basis of relative chronology criteria (i.e., superposed geometries). Statistically, the N160-N10 structures are regarded as the youngest fault system, while the N40-N50 structures are the oldest. According to many authors, the N120-N140 and N90-N110 structures are synchronous, have been generated under a transtensive regime, and are presently active. Many studies (Bouysse, 1979; Bouysse and Westercamp, 1990; Feuillet et al., 2002, 2004; Corsini et al., 2011; Lardeaux et al., 2013; De Min, 2014; Legendre et al., 2018; Legendre, 2018; Verati et al., 2018; Navelot et al., 2018; Favier et al., 2019) have emphasized the importance of structural heritage, and thus tectonic reactivation, on the present-day active deformation pattern. Interestingly, the active Bouillante geothermal field (Figure 1-B) is located at an intersection between three of the main regional tectonic structures (Calcagno et al., 2012, 2015, Figure 1-C).

2-3- Terre-de-Haut in Les Saintes Islands

Terre-de-Haut, the oldest volcanic complex in the Les Saintes Islands, predominantly consists of calk-alkaline lavas, debris and pyroclastic flows, with abundant lava domes and volcanic plugs (Jacques and Maury, 1988; Verati et al., 2016). All volcanic rocks are frequently fractured and deformed by superposed fault systems. We have recently clearly established the main characteristics of the finite brittle field on Terre-de-Haut Island (Verati et al., 2016; Navelot et al., 2018; Favier, 2019). In summary, our structural analyses revealed the existence of four main directions for the orientation of fault networks characterized by the following statistical structural directions: N030-N060-, N070-N100-, N120-N140- and N170-N010-trending fault systems (Figure 2-B). All these faults are generally strongly dipping, and when kinematic criteria are visible, they are compatible with normal faulting with a strike-slip component. This brittle finite strain pattern is therefore consistent with the regional

transtensive tectonic framework currently recognized in the Guadeloupe archipelago (Feuillet et al., 2002, 2004, 2010; Calcagno et al., 2012; Baird et al., 2015; De Min et al., 2015; Leclerc et al., 2016).

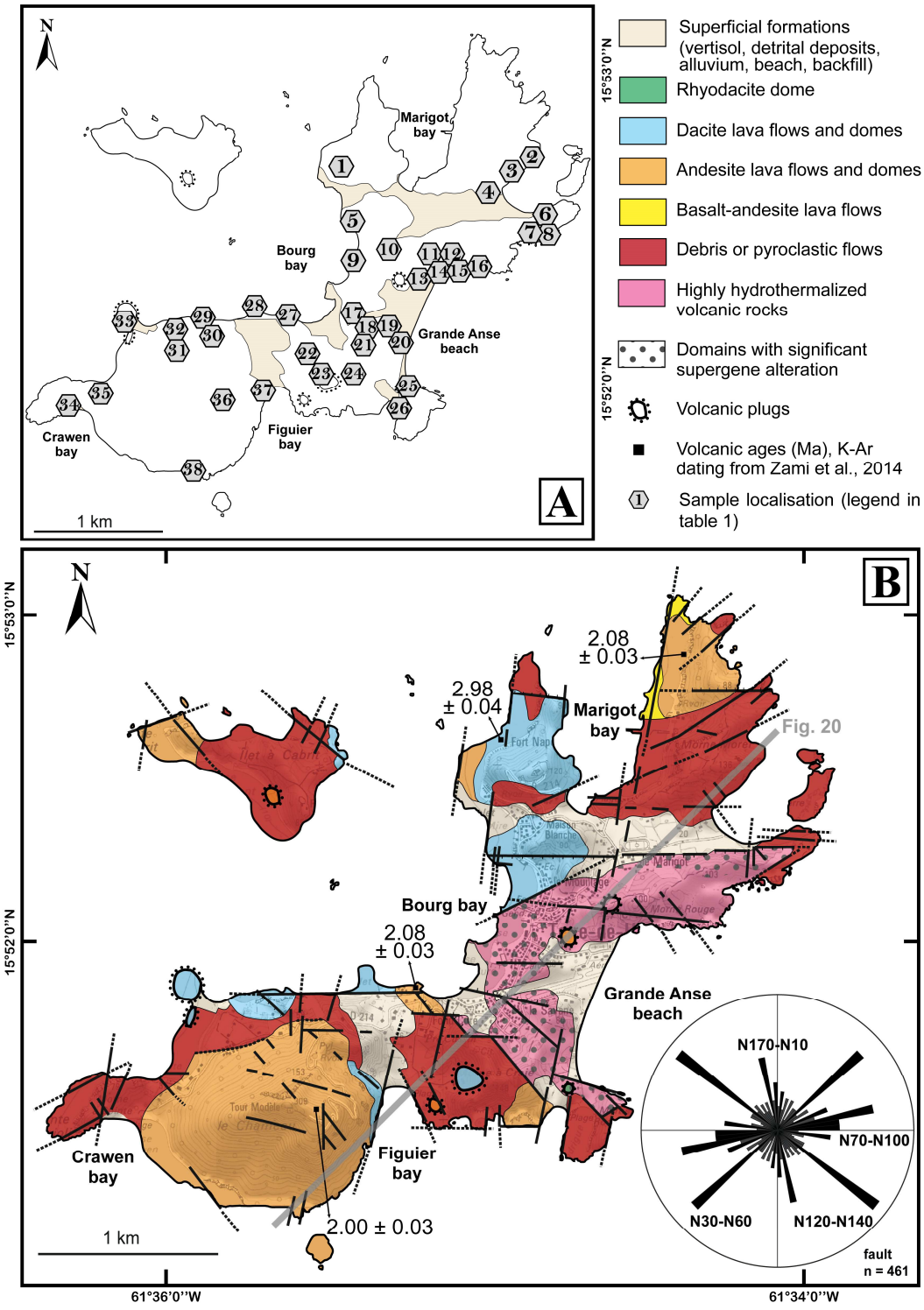

Figure 2: A) Sample localisations map, legend in table 1. B) Revised geological map of Terre de Haut Island showing the main geological formations and the volcanic lithologies defined by their geochemistry and their mineralogy (modified after Jacques and Maury, 1988 and

159 Verati et al., 2016). The heavy dark lines represent the main brittle faults identified in the field
160 (modified after Verati et al., 2016 and Navelot, 2018). **(COLOR / IMAGE SIZE: FULL PAGE)**
161

162 Table 1: Samples location from Terre-de-Haut Island. **(BLACK AND WHITE / IMAGE SIZE:**
163 **COLUMN WIDTH)**
164

Localisation (fig. 2-A)	Samples
1	17TH26
2	17TH28
3	TH-23a,b,c,d,e
4	17TH29
5	TH-30a1,a2,b ; 16STH33
6	TH-32a,b, TH-33
7	GD-16-10
8	17TH30
9	17TH32a,b
10	17TH31
11	SA-14
12	17TH33
13	16STH01a,b; 16STH02; 16STH03; 16STH04a,b; 16STH05; 16STH06; GD16-06
14	16STH07; 16STH08; 16STH09a,b; 16STH10; GD-16-03; GD16-05
15	16STH11a,b; 16STH19; 16STH20; TH26a,b
16	16STH12; 16STH13; 16STH14; 16STH15a,b; 16STH16; 16STH17; 16STH18; 17TH16; 17TH17a,b; TH-27
17	16STH34; GD15-142
18	16STH35a,b; TH-24a,b,c; TH-25
19	17TH01; 17TH02
20	17TH03; 17TH04; 17TH15; 16STH21a,b
21	17TH14; 16STH22
22	17TH12
23	17TH11
24	17TH09; 17TH10
25	17TH05; 17TH06; 17TH07; TH-25'; SA-12-08; GD-17-08
26	17TH08; GD17-09
27	16STH23a,b
28	16STH24; 16STH25; 16STH26; 16STH27; 16STH28
29	16STH30; 16STH31; 16STH32
30	16STH29; 17TH24; TH-28
31	17TH23
32	17TH22
33	17TH21
34	17TH18; 17TH19
35	17TH20

36	17TH25a,b; DC-10-09a,b; GD17-11
37	17TH13; TH-29; GD-15-135
38	GD-15-139; GD15-140; GD15-141

The central part of Terre-de-Haut Island is dominated by a large area (2 km²) of intensely hydrothermally altered rocks (Figure 3), within which the initial magmatic structures and mineralogy have been completely erased, making it impossible to distinguish between lava, debris or pyroclastic flows (Jacques and Maury, 1988; Verati et al., 2016). The recognition of high-temperature hydrothermal mineral associations as well as the importance of fault networks led Verati et al. (2016) to interpret this hydrothermal zone as an exhumed paleogeothermal reservoir. Such hypothesis is consistent with the age of volcanic activity (3-2 Ma) combined with the fact that the Guadeloupe archipelago is subjected to intense weathering and erosion processes (Dessert et al., 2015). Indeed, because effective mechanical and chemical erosion rates are approximately 1-2 mm/yr (Sak et al., 2010; Lloret et al., 2011; Rad et al., 2013; Ricci et al., 2015 a, b), the central part of this island was potentially burried by a minimum of 2 km of volcanic materials. Low-temperature mineral associations typical for subsurface zones of geothermal fields have been recently described in this area (Beauchamps et al., 2019). Altogether, these data suggest that the Terre-de-Haut hydrothermal system is the key target to study an exhumed analogue of a geothermal reservoir in the Guadeloupe archipelago.

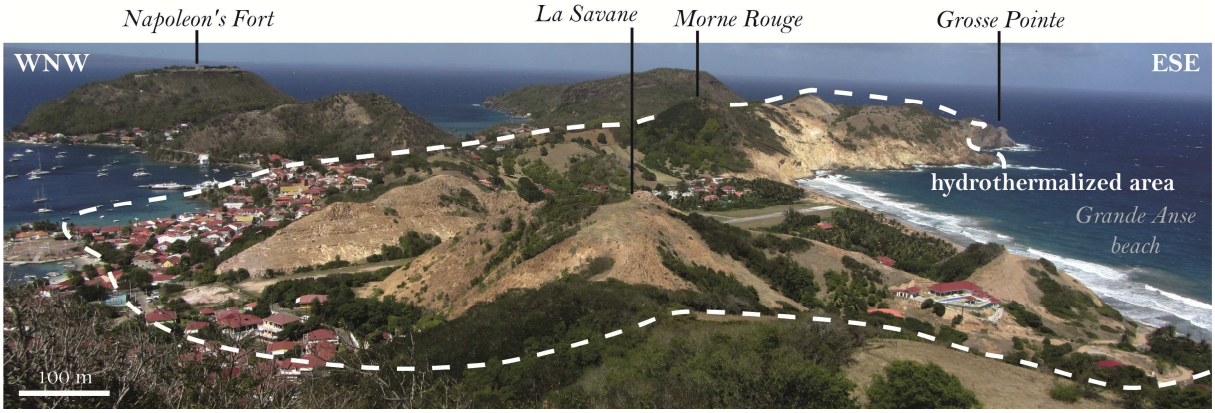

Figure 3: Aerial view of a central portion of the Terre-de-Haut Island showing the extent of the highly hydrothermalized area. View from Pré Cassin. **(COLOR / IMAGE SIZE: FULL PAGE WIDTH)**

3- Material and methods

3-1- Terminology

The term “hydrothermal processes” strictly refers to the changes that occur when fluids circulate into and react with surrounding pre-existing rocks, producing physicochemical changes in these “country rocks” (see reviews in Meyer and Hemley, 1967; Guilbert and Park, 1986; Pirajno, 2009). Because a hydrothermal system requires a heat source, a fluid phase (supergene and/or hypogene fluids) and a transfer structure, there are different geological settings favourable for hydrothermalism. Consequently, the terms relevant to describing the chemical and mineralogical changes in rocks affected by hydrothermalism are not homogeneous. In particular, these chemical/mineralogical transformations are called “hydrothermal alteration” in the geothermal community but are described as “hydrothermal metamorphism” by endogenous petrologists, even if the pioneering and seminal works of Ramberg (1952) and Korzhinskii (1965) established that the physicochemical processes driving the fluid–rock interactions obey similar thermodynamic and kinetic laws. Since the late 2000s (Smulikowski et al., 2007), the International Union of Geological Sciences (IUGS) recommends using the term “hydrothermal metamorphism” for mineralogical and textural transformations of a local extent caused by the circulation of hot H_2O-rich fluids developed in specific settings such as ocean-floor spreading centres, contact aureoles around igneous intrusions, or volcanic/magmatic arcs (see also Fyfe et al., 1978; Mason, 1978; Schiffman et al., 1986, 1991; Liou et al, 1987; Yardley, 1989; Frey and Robinson, 1999). During hydrothermal metamorphism, as is the case in geothermal systems or ore deposit formation, the percolation of volatile and sometimes overpressurized fluids may dissolve and remove chemical elements from the country rocks, significantly altering the country rocks’ chemical composition (Schiffman et al., 1984; Yardley and Cleverley, 2015, with references therein).

As underlined by Schiffman et al. (1984) and Pirajno (2009), high-temperature hydrothermal alteration and hydrothermal metamorphism are terms describing similar processes. Consequently, the term “hydrothermal alteration”, hereafter used, must be considered in its broadest acceptance.

3-2- Mapping lithology, structural analysis and sampling strategy

We mapped the various volcanic units distinguishing the following formations: well-developed soils, superficial quaternary sedimentary formations, debris flows, lava flows, lava domes and volcanic plugs.

More than a hundred measurements across the island of tectonic structures were acquired for this study during seven fieldwork campaigns between 2010 and 2017 to characterize the superposed finite ductile strain fields, the chronology of deformations and, when possible, the kinematics of deformation.

To assess the intensity and degree of hydrothermal alteration of the volcanic rocks, we sampled fresh, slightly altered, and highly altered volcanic rocks. The sampling was executed while taking into account the rock deformation in the regional finite deformation gradient. As a result, the undeformed fresh volcanic rocks are considered a standard reference in order to quantify the effects of hydrothermalism and deformation.

3-3- Whole rock geochemistry

Whole rock major and trace element analyses were performed on 108 samples (localized in figure 2-A and table 1; analytical results provided in the supplementary data in table A-1), first, to improve the definition of the lithotypes defined on the geological map and, second, to specify the magmatic characteristics of the sampled lava flows. We carefully selected the rock exposures to ensure that the main types of lava flows were sampled. Analyses were obtained by using inductively coupled plasma atomic emission spectrometry (ICP-AES) and inductively coupled mass spectrometry (ICP-MS) for major and trace elements, respectively,

239 on rock powders at the Geochemical and Petrographic Research Center in Nancy (SARM
240 laboratory, CNRS-CRPG, with the procedure proposed by Carignan et al., 2001).

241 **3-4- Mineral chemistry**

242 In order to precise and quantify the mineralogical evolution of Terre-de-Haut, we investigated
243 126 thin sections. Mineral chemistry data were obtained by electron microprobe analyses, X-
244 ray diffractometry and Raman spectrometry.

245 Non-oriented powders of whole rocks (<70 µm) were analysed by an X-ray diffractor with an
246 XPert-Pro MPD system (Bragg Brentano geometry, Cu anticathode, KAlpha1 and KAlpha2
247 rays, PIXcel detector) at the CEMEF in Sophia-Antipolis Scientific Center.

248 Mineral major compositions were analysed using the “Service Commun de Microsonde” of
249 the University of Montpellier using a Cameca-SX100 electron microprobe. The operating
250 conditions were a 20 kV accelerating voltage and 10 nA beam current. The chemical
251 analyses of hydrothermal phases are presented in the supplementary data in tables A-2, A-3,
252 and A-4.

253 We also used Raman spectrometry to complete the mineral determination. The spectra were
254 recorded with a LabRam HR800UV Jobin-Yvon™ microspectrometer equipped with 1800
255 g/mm gratings and using 532 nm green laser excitation; the acquisition time span varied from
256 20 to 70 s during three accumulating cycles.

257 **3-5- P-T-XH_2O estimates for hydrothermal mineral associations**

258 The pressure and temperature conditions of hydrothermalism were quantified by the use and
259 the comparison of:

260 - Stability fields of typical geothermal minerals, using the available detailed descriptions of
261 phase distribution with respect to measured temperatures and depths in active geothermal
262 fields (see, for example, Reyes, 1990 and White and Hedenquist, 1995).

- Classical chlorite solid-solution thermometry, which has been successfully used (Lanari et al., 2014) since the pioneering works of Cathelineau and Nieva (1985) and Cathelineau (1988) in both geothermal and low-grade metamorphic systems.

- Thermodynamic modelling of representative samples using the THERIAK-DOMINO method (De Capitani and Petrakakis, 2010) with the Holland and Powell database (1996-2007). These calculations were carried out only on samples not affected or poorly affected by supergene alteration. THERIAK-DOMINO, similar to other mineral equilibrium modelling methods (for example THERMOCALC, Powell et al., 1998), allows us to approach, as closely as possible, the effects of all major chemical elements measured (i.e., real and effective whole rock chemistry) in a given bulk rock composition on the stability of the observed mineral assemblage in the thin section of interest. THERIAK-DOMINO is a free energy minimization program, taking into account available mixing models for mineral solid solutions and allowing calculation of pseudo-sections (i.e., isochemical phase diagrams) for a selected natural sample. Pseudo-section calculations allow exploration of not only the P-T stability fields of complex mineral assemblages (including the relative abundances of the different phases in a given mineral assemblage) but also the effects of the Fe-oxidation state on mineral stabilities as well as the influence of the amount and nature of fluids (particularly H_2O) on the stability field of a given mineral association.

4- Diversity of lithologies

The first geological map of Terre-de-Haut was produced in the 1980s (Jacques and Maury, 1988) and was later improved by geochronological and structural investigations (Zami et al., 2014; Verati et al., 2016). To continue the refinement of Terre-de-Haut geology we produced a revised geological map (Figure 2-B). We refined the definition of volcanic rocks, sampled in domes or lava flows, by systematic geochemical and petrographic investigations taking into account their degree of hydrothermal alteration overprint.

SiO_2 content ranges from 54 to 67 wt.% (100% anhydrous) for lava flows, with a compositional range from basalt-andesite to dacite (Figure 4-A). The studied samples have a calk-alkaline affinity with an evolution from andesites to dacites and medium to low K series (SiO_2 versus Nb/Y diagram, Winchester and Floyd 1977, and K_2O versus SiO_2 diagram, Peccerillo and Taylor 1976, in supplementary data in figure A-1).

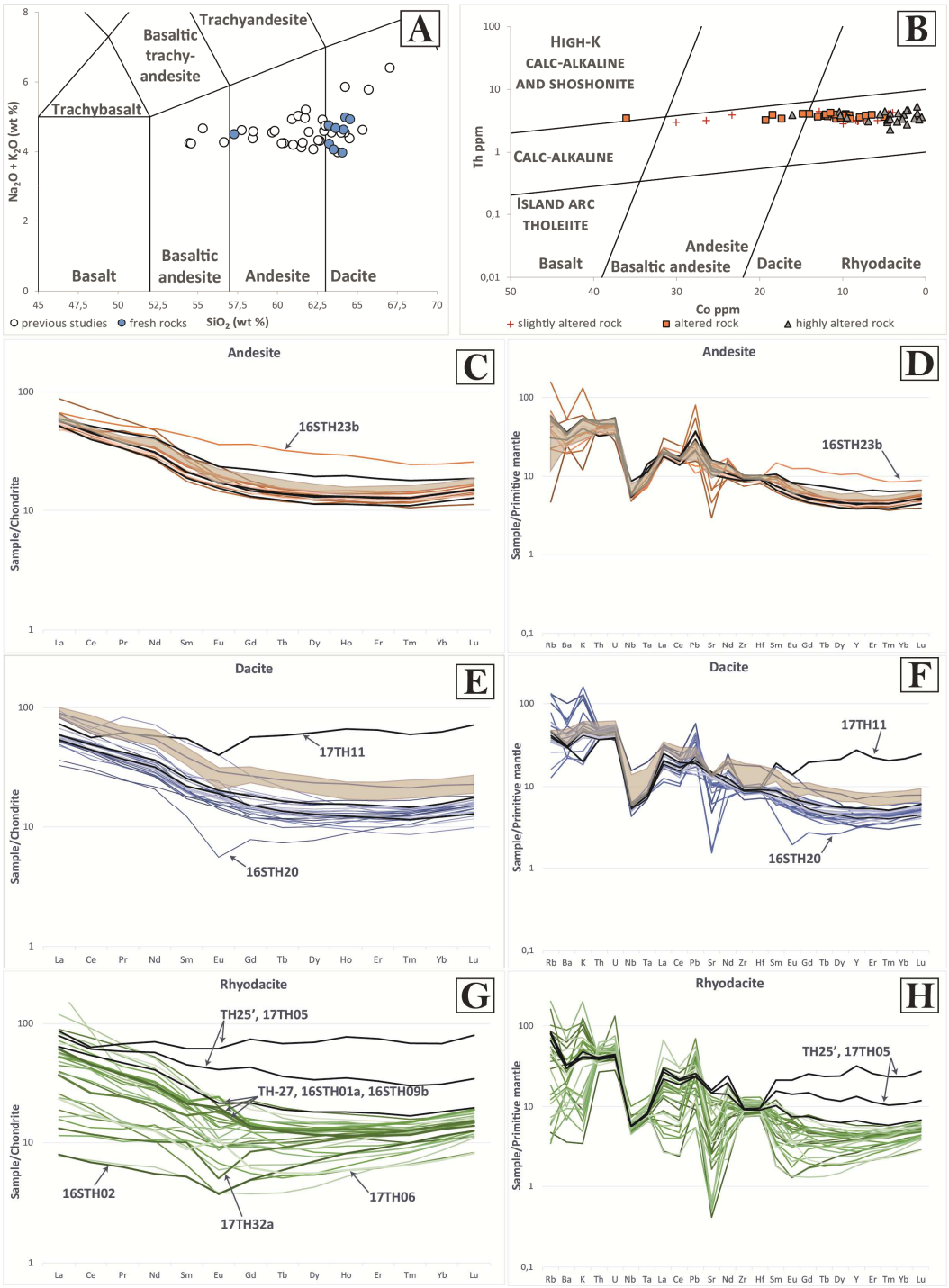

Figure 4: Geochemical characterization of lava flows: A) Total alkali vs. silica diagram after Bas et al. (1986), white circles represent previous data from: Jacques et al., 1984; Jacques and Maury, 1988; Zami et al., 2014 and Navelot et al., 2018. Blue circles correspond to our new analyses. B) Co vs. Th plot after Hastie et al., 2007 showing the primary volcanic chemical characters of the studied rocks whatever their degree of alteration. B, E and G) Rare Earth Element (REE) patterns normalized to chondrite values (after Sun and McDonough, 1989) of the andesite, dacite and rhyodacite lava flows, respectively, used in this study. D, F and H) Multi-element patterns normalized to primitive mantle (after Sun and McDonough, 1989). For C to H : The shaded bands correspond to the range determined for Terre-de-Haut volcanic rocks (after Zami et al., 2014) and black bold lines for fresh samples. **(COLOR / IMAGE SIZE: FULL PAGE WIDTH)**

The Rare-Earth-Element (REE) diagram normalized to chondrite values (after Sun and McDonough, 1989; Figures 4-C, E and G) displays relatively constant slopes with light REE (LREE) enrichment for most samples, which is typical of insular arc-related calk-alkaline lavas (Hawkesworth and Powell, 1980; Labanieh, 2009). Moreover, the multi-element diagram normalized to primitive mantle (Sun and McDonough, 1989; Figure 4-D, F and H) also displays typical patterns of calk-alkaline arc lavas, i.e., with Th, Pb, U and large ion lithophile element (LILE) enrichments and Nb and Ta negative anomalies (Labanieh, 2009).

The rhyodacitic samples (Figures 4-G and H) show the most diversified geochemistry with especially strong Sr depletion, large K, Th, U enrichments, or K depletion. This geochemical variability can be explained either by different magmatic differentiation stages or by element mobility during alteration processes, especially for Sr and K.

However, the positive Y and heavy-REE (HREE) anomalies of samples from “Morne à Craie” (17TH11) (Figure 4-F) and the intrusion in the southern part of Grande Anse beach (TH-25’ and 17TH05, Figure 4-H) reflect supergene processes (Cotton et al., 1995), as also identified in REE spectra (Figures 4-E and G).

Major and some trace elements (mainly LILEs and LREEs) are severely mobile in altered lavas. Therefore, to improve the geochemical characterization of our samples, particularly those affected by hydrothermal transformations, we selected diagrams based only on minor and trace elements considered the most immobile. Samples where the LOI (loss on ignition) is below 1-2% and in which the primary volcanic mineralogy is well preserved (see section 6), demonstrating that hydrothermalism and/or weathering are insignificant, are named

slightly altered rocks, while when the LOI is above 3% (as suggested by Samper et al., 2007, to identify significantly altered volcanic rocks), and when secondary minerals are abundant, they are named altered or highly altered rocks. Hypogene and supergene hydrothermal alteration produce new mineral assemblages often associated with significant redistribution of chemical elements (Sturchio et al., 1986; Fulignati et al., 1999; Pandarinact et al., 2008; Salaün et al., 2011). For these reasons, we used the Th-Co diagram proposed by Hastie et al. (2007), which is an efficient tool for the characterization of magmatic protolith signatures in altered lava flows. In this diagram, the studied rocks define a typical medium-K calk-alkaline volcanic series (Figures 4-A and A-1) characterized by significant magmatic differentiation from basaltic andesites to rhyodacites. Many lava domes and volcanic plugs correspond to andesites or rhyodacites. Lava flows are more diversified and thus we distinguished, on the revised geological map, basalt-andesites, andesites, dacites and rhyodacites (Figure 2-B).

In common trace element diagrams (Figures 4 C to H), the lava flow samples are compared to fresh volcanic rocks from Terre-de-Haut Island (Zami et al., 2014)

Hydrothermally altered andesite samples (Figures 4-C and D) are similar to fresh volcanic andesites. A specific sample (16STH23b) displays enrichment in MREEs (middle-REEs) and HREEs, typical for weathering and leaching processes (Zhou et al., 2013).

Dacite samples (Figures 4-E and F) display a consistent trend for most samples with enrichment in LREEs. However, two samples (17TH11 and 16STH20) show chemical anomalies indicating supergene alteration processes (Cotten et al., 1995; Zhou et al., 2013; Ricci et al., 2017) and plagioclase fractionation or interaction with mildly acidic low temperature fluids (Bau, 1991; Taylor and McLennan, 1995) respectively.

Rhyodacite samples (Figures 4-G and H) display the most varied spectra with different degrees of LREE enrichment. This feature can be either related to different magmatic differentiation stages or to secondary alteration events (hydrothermal and/or supergene

alteration). Some samples show especially negative or positive Eu anomalies, suggesting either plagioclase fractionation or interaction with secondary fluids (Bau, 1991). For example, two severely hydrothermalized samples from the southern part of the Bourg Bay area (17TH32a) and the northern part of Grande Anse beach (16STH02) reveal both LREE depletion and slightly negative Eu anomalies related to typical high temperature alteration under mildly acidic conditions (Bau, 1991). Other hydrothermalized samples from the northern part (TH-27, 16STH01a, 16STH09b) and southern part (17TH06) of Grande Anse beach present a positive Eu anomaly due to acidic high-temperature hydrothermal fluids (Michard et al. 1983; Cotten et al., 1995). Samples from the southern part of Grande Anse beach (TH-25' and 17TH05) show high HREE enrichment and slight negative Ce anomalies, reflecting weathering processes under tropical conditions (Cotten et al., 1995; Zhou et al., 2013; Ricci et al., 2017), as already observed for the dacitic sample (Figure 4-E).

5- Structural and microstructural analyses

Despite previous structural analyses at Terre de Haut (Jacques and Maury, 1988; Verati et al., 2016; Navelot et al., 2018), we identify for the first time in Terre-de-Haut Island zones of ductile deformation (Figures 5-A and B), marked by the development of spaced cleavages produced by pressure-solution processes.

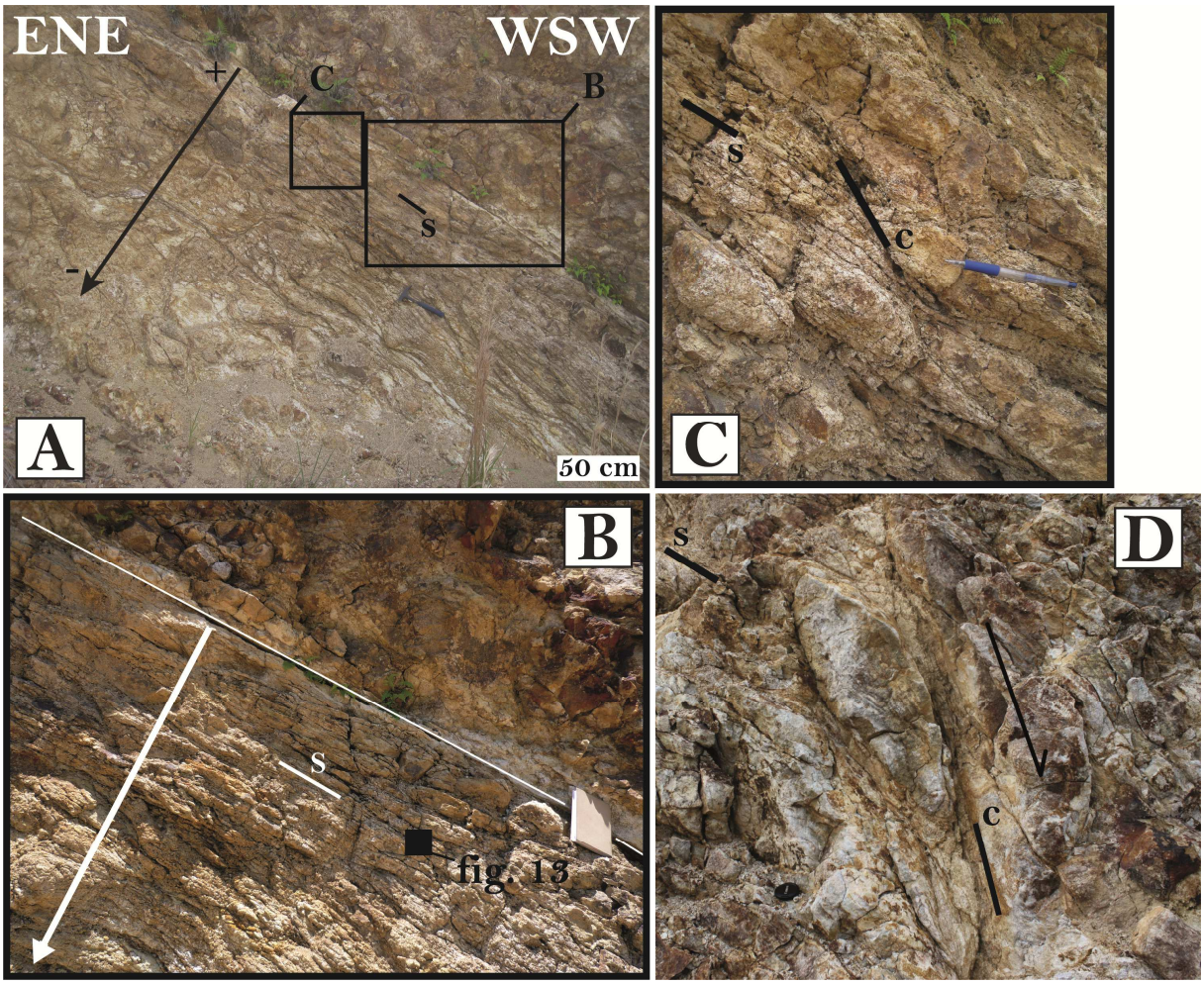

Figure 5: A) Schistose corridors showing a finite deformation gradient (from the aerodrome quarry). B) Zoom on well-developed schistosity planes. C) Local ductile strain pattern with S (schistosity) and C (shear planes) structure compatible with normal sense of shear (schistosity plane N160, 40W, stretching lineation N270, 35W, C plane N0, 75W). D) Typical S (schistosity) and C (shear planes) structure compatible with a normal sense of shear in the area of interest. **(COLOR / IMAGE SIZE: FULL PAGE WIDTH)**

These planar rock structures are concentrated into decametre to hectometre corridors and thus define “ductile shear zones” within the finite ductile strain pattern (Figures 5-A and B and Figures 6-A and B). Stretching lineations are difficult to decipher, but in highly strained domains, strongly dipping lineations and local C/S or C’ structures indicate a normal sense of shear (Figures 5-C and D). At both the outcrop and map scales (Figures 7-A and B), the shear zones are heterogeneously distributed and tend to anastomose, forming lenticular pods (Figure 6-A and sector 1 in Figure 7-A) or producing high-angle intersections (Figures 6-B and sector 2 in Figure 7-B).

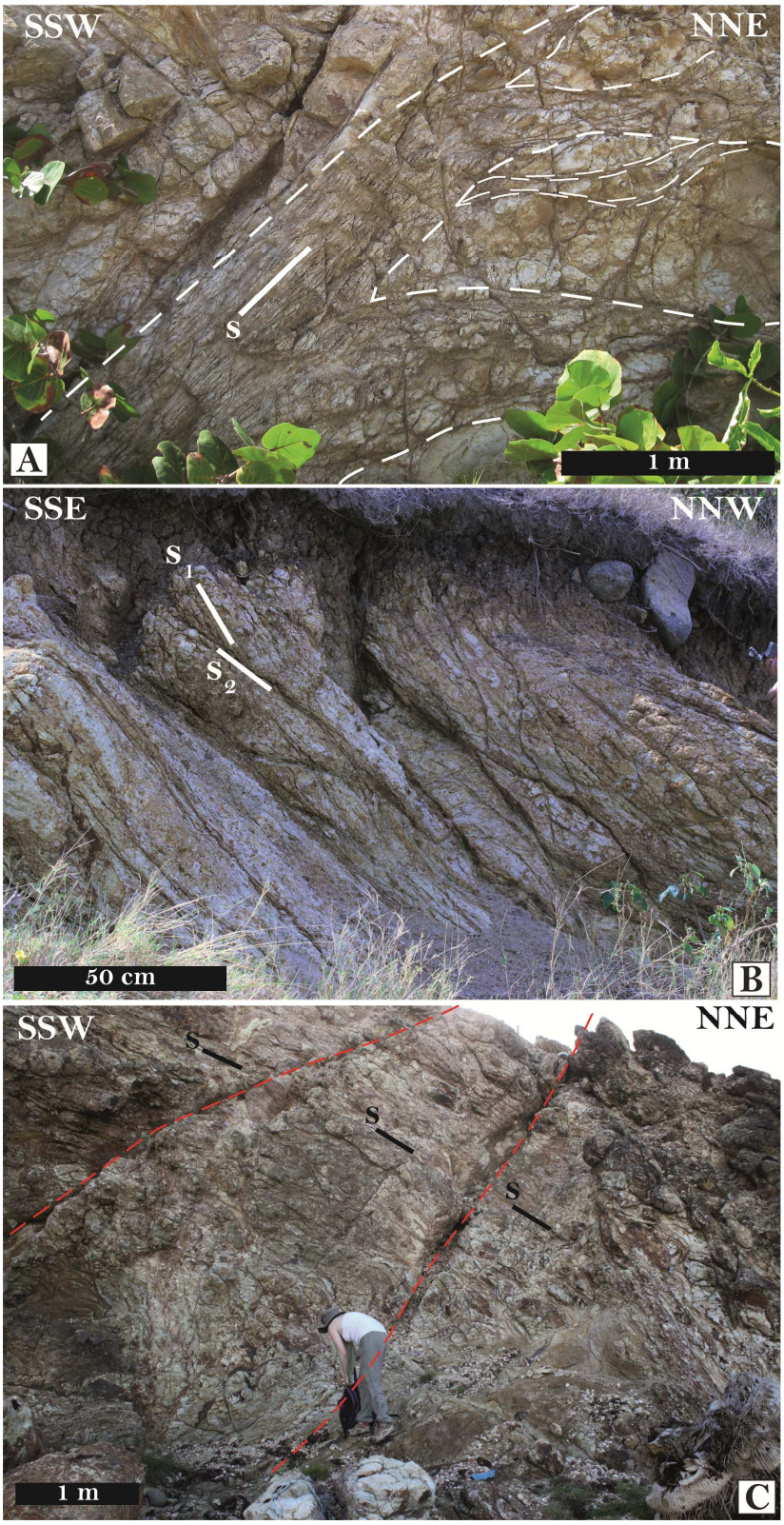

Figure 6: A) Anastomosing schistosity planes forming lenticular pods. Outcrop from La Savane. B) Intersection between two schistosity planes. Outcrop from north of Chameau dome. C) Schistosity plane (S) intersected by fault planes (red dotted lines) and fractures. Top of La Savane outcrop. **(COLOR / IMAGE SIZE: FULL PAGE WIDTH)**

392 Four directions of ductile shear zones (Figure 7-A) have been observed and measured in
393 the field: (1) N020-N060, (2) N120-N140, (3) N070-N100, and (4) N150-N180. Both the
394 abundance of anastomosed structures and the absence of coherent and repetitive criteria of
395 relative chronology within the superimposed geometries (i.e., intersections) lead us to
396 propose that the observed finite geometries are synchronously developed during progressive
397 deformation.

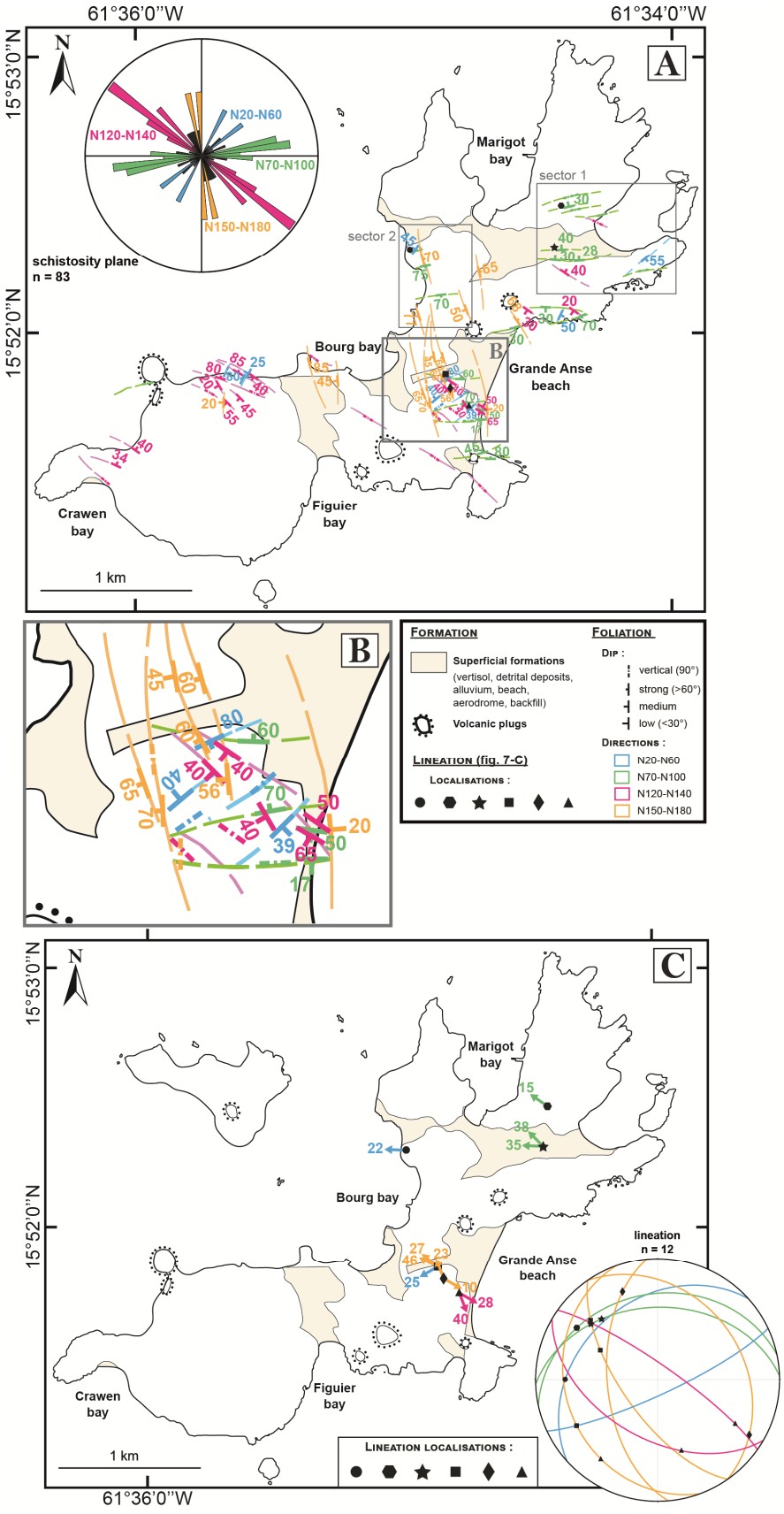

398

399 Figure 7: A) Tectonic sketch map of schistosity trajectories on Terre-de-Haut Island. B) Zoom
400 on central part of Terre-de-Haut Island. C) Map of measured lineations on the Terre-de-Haut
401 Island. **(COLOR / IMAGE SIZE: FULL PAGE WIDTH)**

The planar fabrics display variable dips from 90 to 10° (Figures 6 and 8), and when observable, the stretching lineations have dips ranging between 10 and 45° (Figure 7-C and Table 2). The lineations' dip is compatible with the occurrence of a strike slip component associated with ductile extensional shearing.

Table 2: Schistosity planes (S) and associated lineations (L) presented in Fig.7. **(BLACK AND WHITE / IMAGE SIZE: FULL PAGE WIDTH)**

Site	Type	Strike	Dip	Quadrant	Trend	Plunge
●	S	N228	35	N		
	L				272	22° W
⬣	S	N258	30	N		
	L				305	15° NW
★	S	N268	40	N		
	L				315	38°NW
	L				272	23° W
■	S	N145	66	W		
	L				310	27° NW
	L				297	46° NW
■	S	N60	80	S		
	L				240	25° SW
♦	S	N175	56	W		
	L				340	23° NW
♦	S	N325	30	E		
	L				120	10° E
▲	S	N120	50	SW		
	L				160	40° S

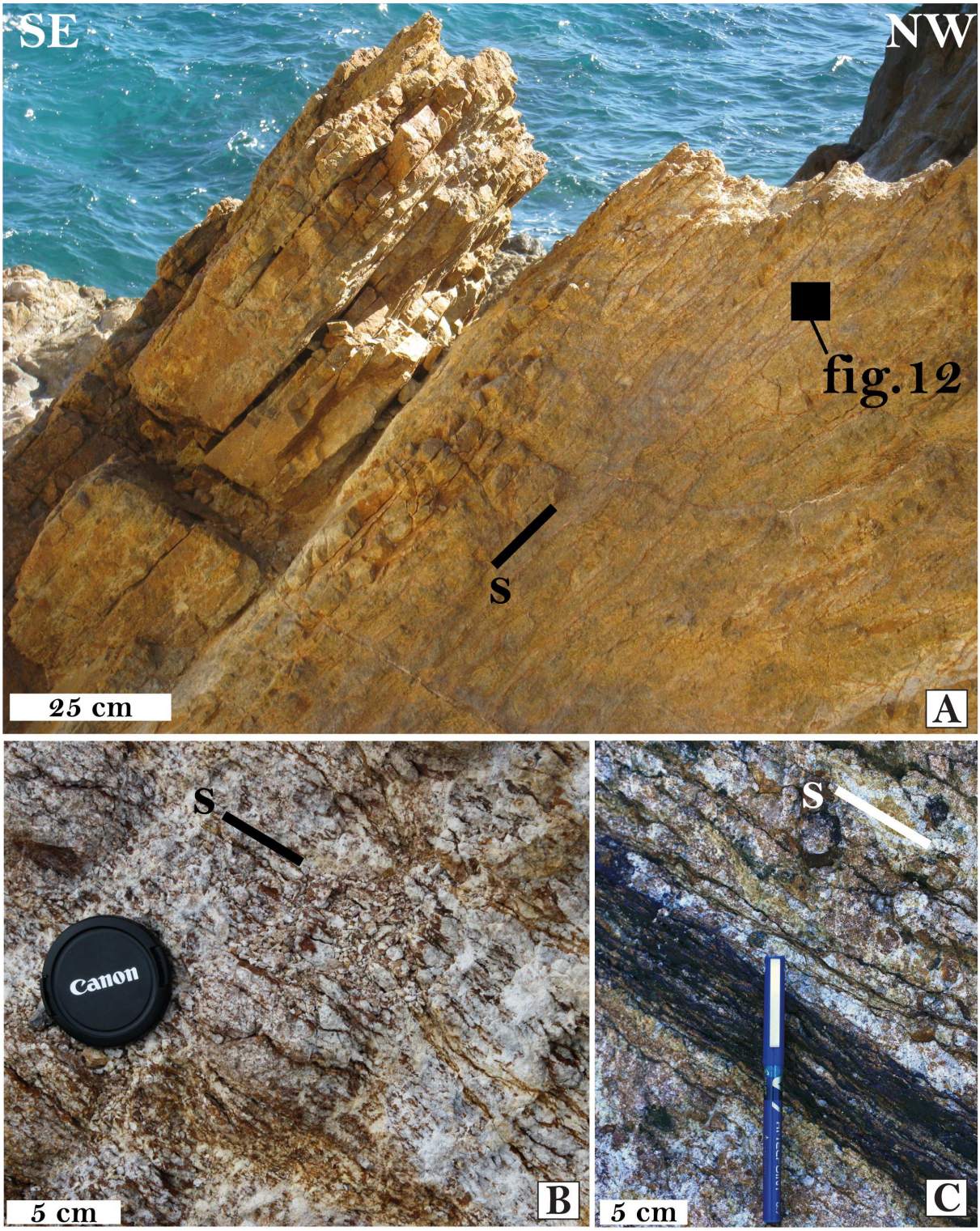

Figure 8: A) Highly hydrothermalized volcanic rock from North of Grande Anse beach with strong dip schistosity plane (S) expressed by spaced disjunctive cleavages. B) Penetrative schistosity plan (S) with low dip, planar fabric underlined by insoluble dark minerals (iron-oxides). C) Example of a penetrative low dip schistosity plan (s) with concentration of insoluble minerals in dark band. **(COLOR / IMAGE SIZE: FULL PAGE WIDTH)**

At the outcrop scale, the observed planar fabric is underlined by dark seams of insoluble dark minerals (iron oxides) and corresponds to well-developed spaced disjunctive cleavages

(Powell, 1979; Borradaile et al., 1982; Rutter, 1983; Neuendorf et al., 2005; Passchier and Trouw, 2005; Brodie et al., 2007; Figure 8). In polymineral rocks, the passive concentration of insoluble minerals attests to stress-driven pressure solution processes (Durney, 1972; Green, 1984), a major mechanism of ductile deformation of the upper crust, which is frequently observed at the brittle/ductile transition zone (see Gratier et al., 2013, with references therein, for an extensive review).

In Terre-de-Haut Island, the spacing of the observed solution cleavage is variable (Figures 5, 6-A-B and 8) and is locally associated with veins or fractures (Figures 6-C and 9-A). Most of the time, the veins or micro-cracks are perpendicular, or at high angles, to the spaced disjunctive cleavages (Figure 9-D).

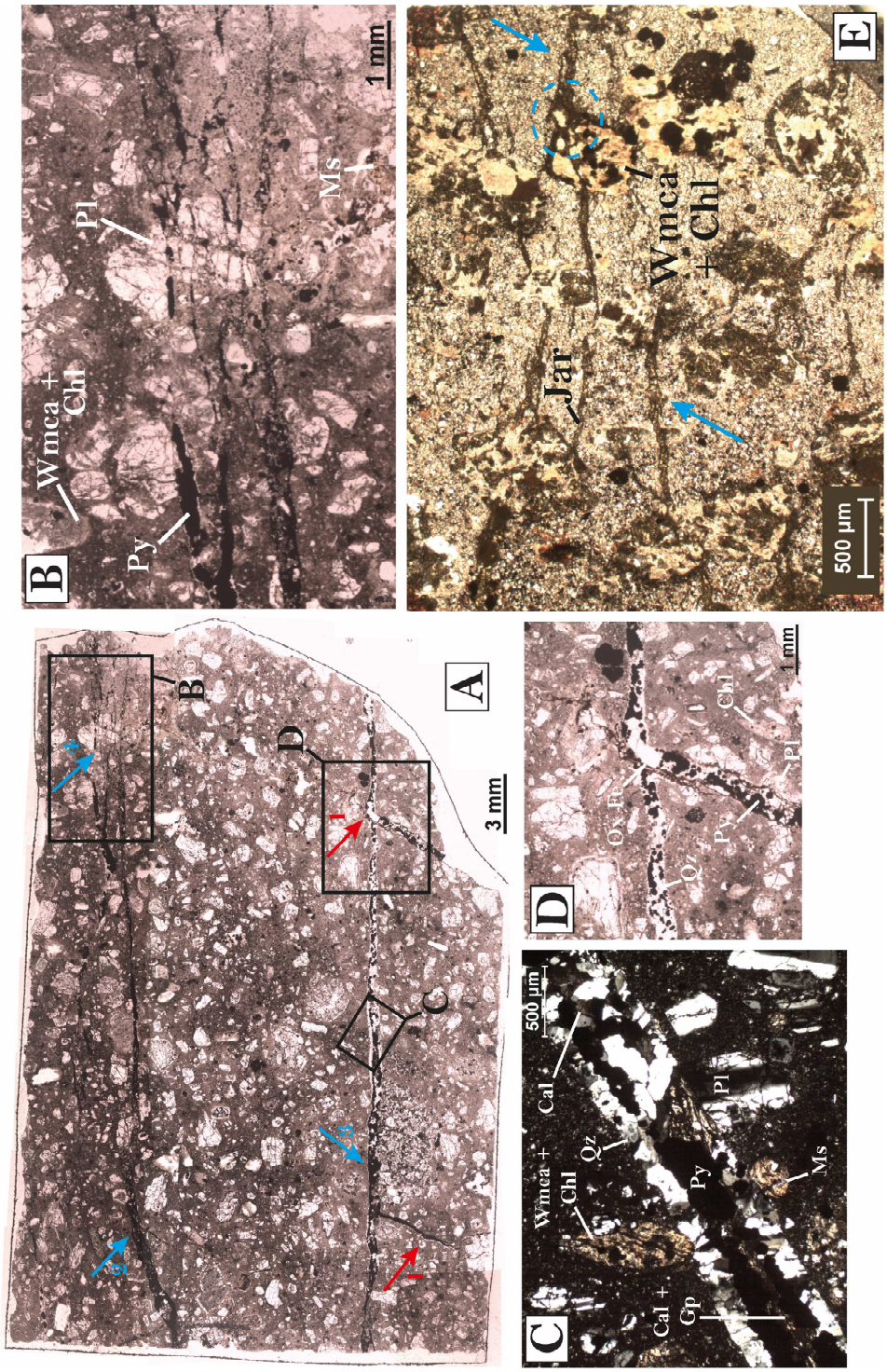

Figure 9: A) Schistosity planes (thin section scale) underlined by insoluble minerals (blue arrows). Schistosity plane reworked by opening of late veins (red arrows). B) Zoom on schistosity planes, underlined by concentration of oxides and pyrite. Pressure-solution cleavage is marked by partial dissolution of volcanic plagioclase. C) Zoom on a vein reworking the schistosity plane and filled with quartz, pyrite, calcite and gypsum. D) Zoom on an intersection of two veins. E) Spaced disjunctive cleavages (blue arrow) underlined by jarosite (Jar). Sample from the aerodrome quarry. Blue arrow indicates schistosity planes with jarosite. Blue dotted circle indicates the intersection between schistosity plane and volcanic mineral replaced by hydrothermal phases (Wmca = white mica; Chl = chlorite). **(COLOR / IMAGE SIZE: FULL PAGE WIDTH)**

In thin-section, the spaced cleavages are also underlined by concentrations of insoluble minerals, such ilmenite and magnetite and also, in a restricted number of cases, by crystallization of pyrites or sulphates (gypsum, jarosite, barite; Figures 9-C and E). The spaced disjunctive cleavages, leading to the concentration of insoluble mineral species, are mostly developed in the volcanic groundmass of lava flows. When volcanic phenocrysts are intersected by spaced disjunctive cleavages, we frequently observe local dissolution of these primary volcanic minerals, mainly at their periphery (Figures 9-B, C and E). Moreover, in such a case, the volcanic phenocrysts, particularly the pyroxenes, are severely pseudomorphosed, with a gradient of alteration from rims to cores, and replaced by a secondary assemblage rich in white micas, chlorites, albite and quartz. Altogether, these microstructural observations confirm first that the observed spaced cleavages are the result of intergranular pressure-solution mechanisms and second that solution cleavage formation is contemporaneous with fluid and mass transfers responsible for hydrothermal alterations of pyroxenes. Moreover, in the studied lavas, as is the case in the whole volcanic arc of the Guadeloupe archipelago, the volcanic groundmass is rich in infra-millimetre microlites (particularly Fe or Fe-Ti), oxides and anorthoclases.

6- Petrography and mineralogy

Because of the heterogeneity of the hydrothermal transformations, the finite deformation state, and finally, the degree of supergene alteration depicted in Terre-de-Haut Island, we need to establish clear petrographic distinctions between fresh, slightly altered, altered, and highly altered volcanic rocks. Mineral chemistry was performed on all rock types, and selected microprobe analyses are presented in table 3 and in supplementary data tables A-2, A-3 and A-4. Except for fresh volcanic rocks, two stages of hydrothermal alterations, and a late stage of supergene alteration, were recognized on the basis of classical microstructural overprinting criteria.

6-1-Fresh rocks

The well-preserved lava flows and volcanic plugs are basaltic andesite, andesite, dacite and rhyodacite. Numerous infra-millimetre microlites of Fe-Ti oxides are present in all lavas, while anorthoclase microlites are also observed in dacites and rhyodacites.

All fresh rocks show porphyric textures with various amounts and natures of phenocrysts depending on the lithology.

- Plagioclases (70-75% of the observed phenocrysts): The phenocrysts are present in all lithologies and are mostly labradorite and less frequently bytownite. As previously underlined by Jacques and Maury (1988), in basaltic andesites and andesites, some plagioclases are zoned, with bytownite in the core and labradorite towards the rim.

- Ferromagnesian phases (20-25% of the observed phenocrysts): Brown amphiboles are observed in basaltic andesites, andesites and dacites, and their compositions vary from hornblende to edenite or pargasite depending on the considered bulk-rock chemistry (cf. Jacques and Maury, 1988). Pyroxenes are presenting all rock types. The orthopyroxenes are hypersthene, while the clinopyroxenes are augite.

- The oxides (5% of the observed phenocrysts), are ilmenite and/or titanomagnetite.

6-2-Slightly hydrothermally altered rocks

In these rocks, the primary volcanic textures are preserved, but we observed the limited development of coronas around ferromagnesian volcanic phases (Figures 10-A and B), mainly around orthopyroxenes and clinopyroxenes. In the coronas, the secondary mineral phases are actinolite, chlorite, muscovite and calcite. The most affected lithologies are dacite and debris or pyroclastic flows, within which the secondary phases represent 5 to 10% of the observed mineral composition.

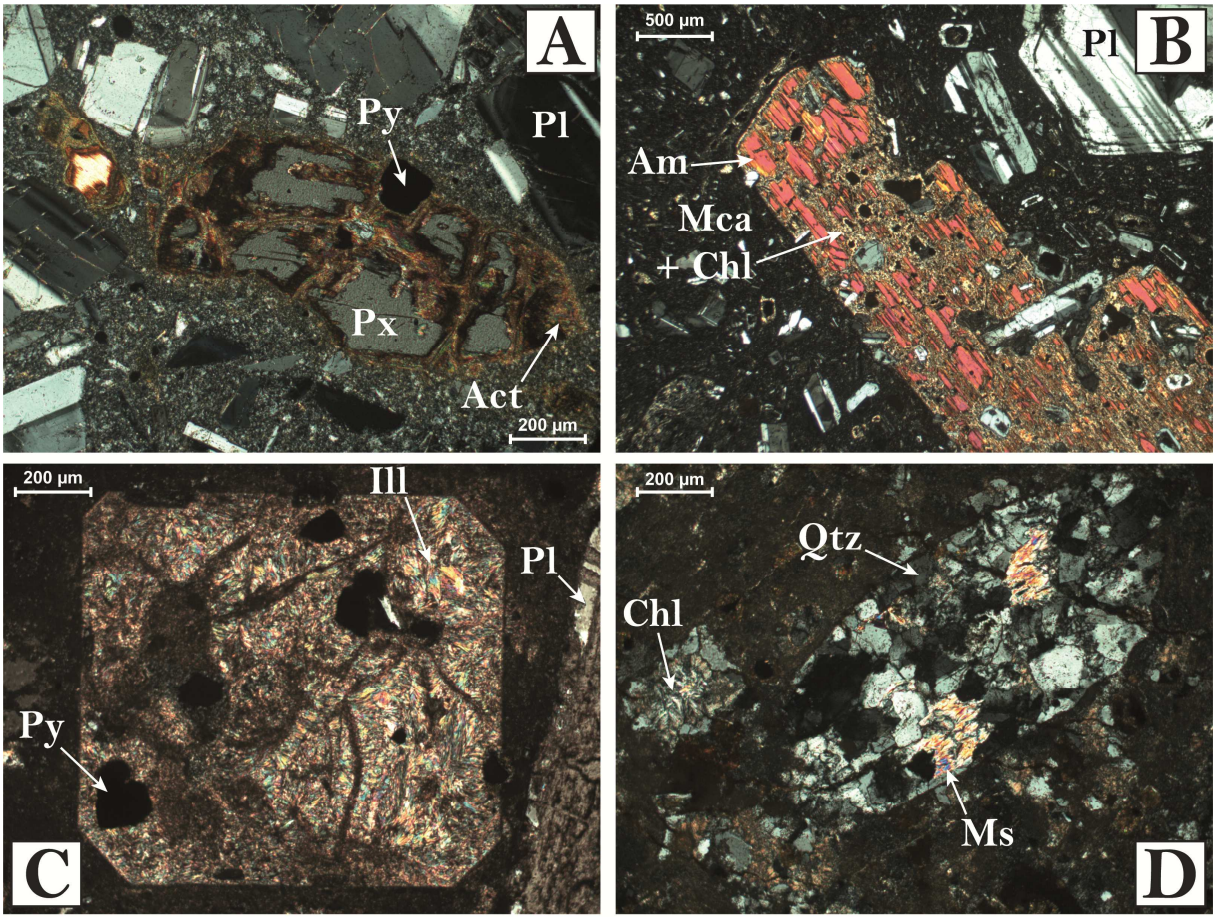

Figure 10: High-temperature (first hydrothermal stage, T above 300°C) pseudomorphic transformations of volcanic minerals. A) Reaction coronas around pyroxene, highlighted by actinolite, in an altered andesite. Sample from south of Bourg bay (16STH23a). B) Replacement of volcanic amphibole by a mix of chlorite and mica, in altered rhyodacite from a pyroclastic flow. Sample from north of Crawen bay (17TH20b). C) Volcanic pyroxene replaced by white mica, in an altered rhyodacite. Sample from north of Grande Anse beach (16STH19). D) Volcanic phase replaced by quartz, chlorite and/or muscovite, in an altered rhyodacite. Sample from La Savane (16STH21a). Act = actinolite, Am = amphibole, Chl = chlorite, Qtz = quartz, Ill = illite, Mca = mica, Ms = muscovite, Pl = plagioclase, Px = pyroxene, Py = pyrite. **(COLOR / IMAGE SIZE: COLUMN WIDTH)**

6-3-Hydrothermally altered rocks

In this category of rocks, we observe relicts of volcanic textures: more than 70% of volcanic pyroxenes or amphiboles and more than 50% of volcanic plagioclases are transformed. The hydrothermal phases can completely replace the initial volcanic phenocrysts (pseudomorphic transformations, Figures 10-C and D), and the most altered lithologies are dacite and rhyodacite lava flows. The observed secondary minerals are quartz, albite, epidote (clinozoisite in small sticks in Figure 11-B and pistacite in colourless grains in Figure 11-E),

muscovite (Figure 11-A), biotite, chlorite (Figures 11-C and D), actinolite (Figure 11-F), titanite (Figure 11-E), and, in a lesser amount, talc (Figure 11-C), and pyrite. In many cases, grey automorphous chlorite grains are rimmed by green-grey to yellow fibrous grains. Subautomorphous muscovites can be replaced by pyrophyllite or fibrous overgrowth acicular crystals in sheaf-like aggregates of illite and green to yellow chlorites (Figure 10-C). In late veins, small-sized cracks or vacuoles, carbonates (microcrystalline calcite grains with polysynthetic twins in Figure 12-A and subautomorphous calcite grains in Figure 11-F), sulphates (Figures 12-B and C), silica polymorphs (quartz, chalcedony, cristobalite, Figure 12-D), acicular or radial zeolites (Figure 12-D and E), and illite in sheaves or spherules can also be observed. Finally, in a restricted number of samples, a strong supergene alteration is marked by the complete transformation of volcanic phases by clay minerals, particularly kaolinite.

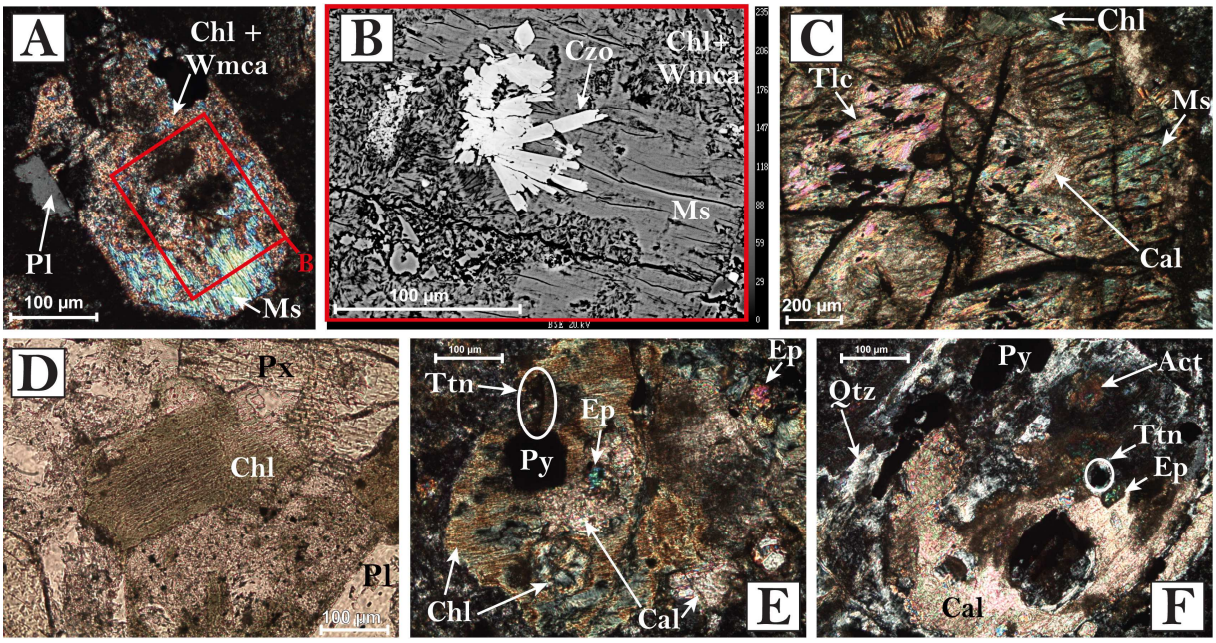

Figure 11: Diversity of secondary new phases developed at the expense of primary volcanic minerals. A) Pyroxene replaced by muscovite and a fine-grained mix of chlorite-white mica, in an altered rhyodacite. Sample from north of Grande Anse beach (16STH16). B) BSE Back-scattered electron image (EPMA acquisition). Zoom on clinozoisite and displaying contrast between fibrous muscovite and the mix chlorite-white mica. C) Volcanic phenocryst pseudomorphosed by multiple secondary new phases, in an altered andesite. Sample from north of Grande Anse beach (SA-14). D) Fibrous green chlorite, in an altered andesite. Sample from north of Grande Anse beach (SA-14). E) Pyroxene phenocryst replaced by numerous secondary new phases, in an altered andesite. Sample from north of Grande Anse beach (SA-14). F) Crystallization of various secondary new phases at the expense of a

volcanic phenocryst, in an altered dacite. Sample from north of Grande Anse beach (17TH16). Act = actinolite, Cal = calcite, Chl = chlorite, Czo = clinozoisite, Ep = epidote, Ms = muscovite, Qtz = quartz, Pl = plagioclase, Px = pyroxene, Py = pyrite, Tlc = talc, Ttn = titanite, Wmca = white mica. **(COLOR / IMAGE SIZE: FULL PAGE WIDTH)**

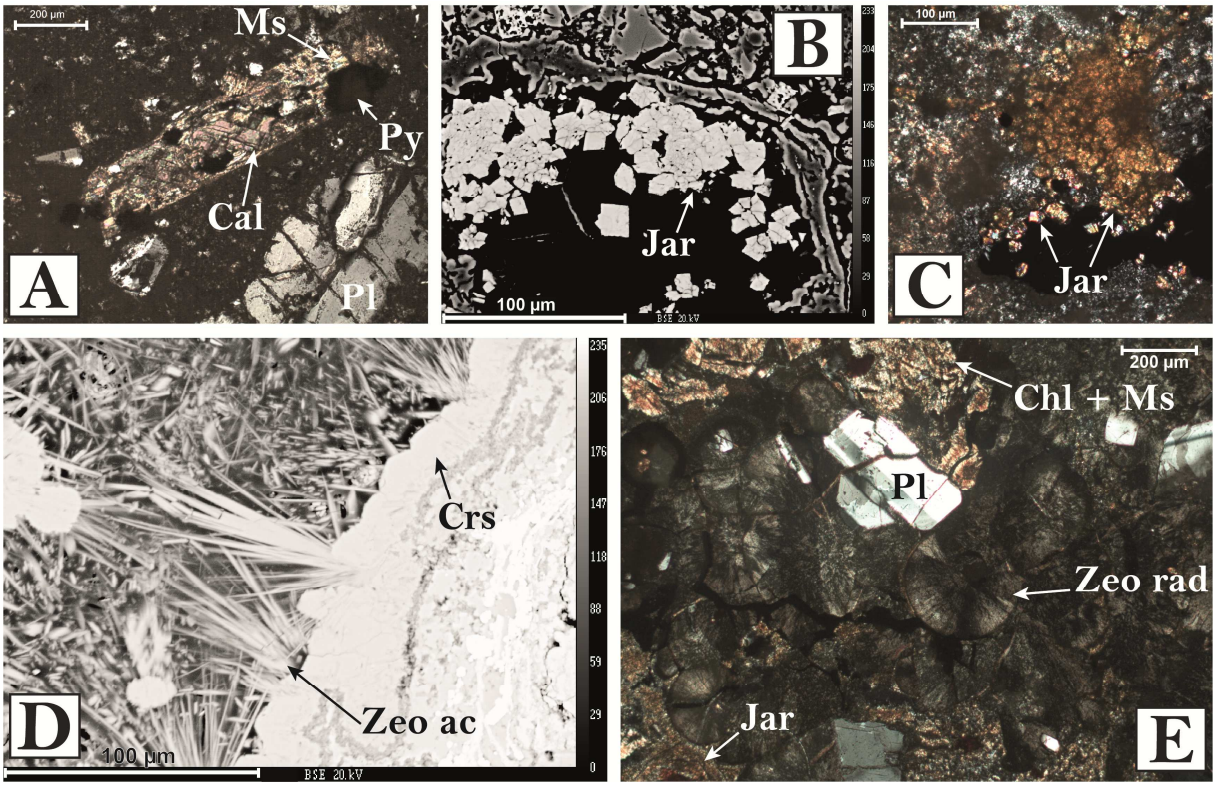

Figure 12: Examples of low-temperature (second hydrothermal stage, 220<T<300°C) mineral crystallizations. A) Ferromagnesian phenocryst replaced by calcite, in an altered dacite. Sample from north of Grande Anse beach (16STH11b). B) BSE image. Jarosite, on the edge of a cavity, in an altered dacite from a pyroclastic flow. Sample from north of le Chameau volcanic dome (17TH24). C) Jarosite on the edge of a cavity, in an altered dacite. Sample from north of Grande Anse beach (16STH20). D) BSE image. Cristobalite and acicular zeolite on the edge of a cavity, in an altered dacite from a pyroclastic formation. Sample from north of le Chameau volcanic dome (16STH29). E) Jarosite and radial zeolite in matrix of an altered dacite from pyroclatic flow. Sample from north of le Chameau volcanic dome (16STH29). Cal = calcite, Chl = chlorite, Crs = cristobalite, Jar = jarosite, Ms = muscovite, Pl = plagioclase, Py = pyrite, Zeo ac = acicular zeolite, Zeo rad = radial zeolite. **(COLOR / IMAGE SIZE: FULL PAGE WIDTH)**

The most hydrothermalized rocks are located in the central part of the island. Here, the primary volcanic textures have been completely erased, and in some cases, phantoms of phenocryst shapes can be recognized. In most cases, the whole rock is recrystallized (phenocrysts and matrix) into a fine-grained association of new phases including quartz-epidote-white micas-chlorite-actinolite-titanite +/- talc.

In the central part of the island, a significant amount of supergene clay minerals, particularly illite-smectite partly altered in smectite, kaolinite and, to a lesser extent, halloysite have been recently recognized and described in detail (Beauchamps et al., 2019). In this area, gypsum and calcite are also frequently observed.

6-4-The different stages of hydrothermalism - a synthesis

Altogether, the microstructural overprinting criteria observed in the Terre-de-Haut hydrothermalized rocks attest to a polyphased hydrothermal alteration history with the following stages:

- A first stage with the mineral association of quartz + albite + epidote + muscovite + grey chlorite (Figures 13-A and B) + biotite + actinolite + titanite +/- talc and pyrite.

- A second stage with the crystallization of illite + green to yellow chlorite (Figure 13-B) + silica polymorphs + pyrophyllite + calcite + sulphates + zeolites.

- A third stage with a supergene mineral association including illite-smectite or smectite + kaolinite + calcite + gypsum +/- halloysite.

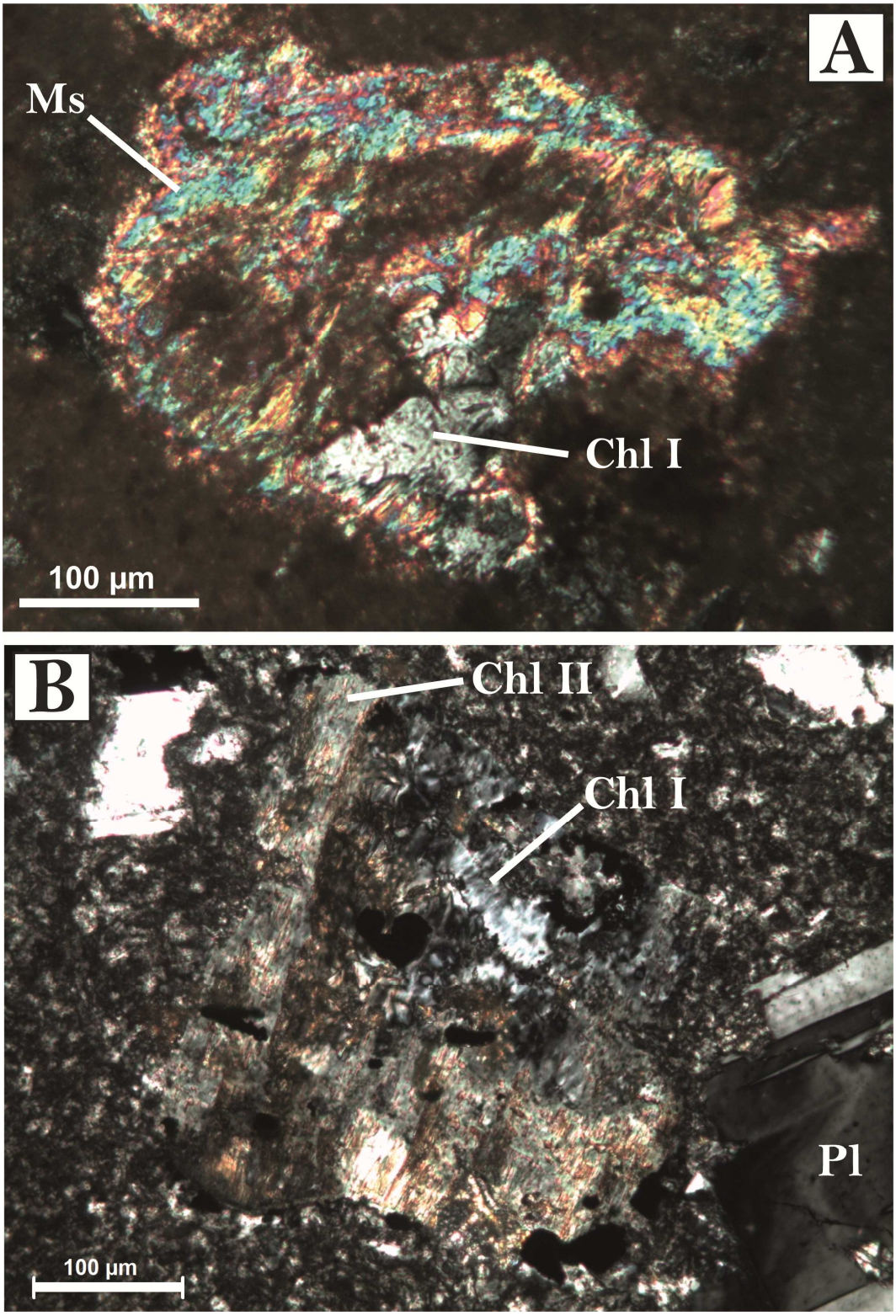

Figure 13: Chlorite morphologies. A) Ferromagnesian phenocryst pseudomorphosed by fibrous muscovite and grey automorphous crystals of chlorite (type I), in a transformed rhyodacite. Sample from north of Grande Anse beach (16STH19). B) Ferromagnesian phenocryst pseudomorphosed by grey automorphous crystals of chlorite (type I) and green-grey to yellow fibrous grains (type II), in a transformed dacite. Sample from north of Grande Anse beach (17TH16). **(COLOR / IMAGE SIZE: COLUMN WIDTH)**

To highlight the importance and spatial distribution of the previously described transformations, we propose a map of mineral occurrences at the scale of Terre-de-Haut Island (Figure 14), distinguishing the two hydrothermal stages and supergene alterations.

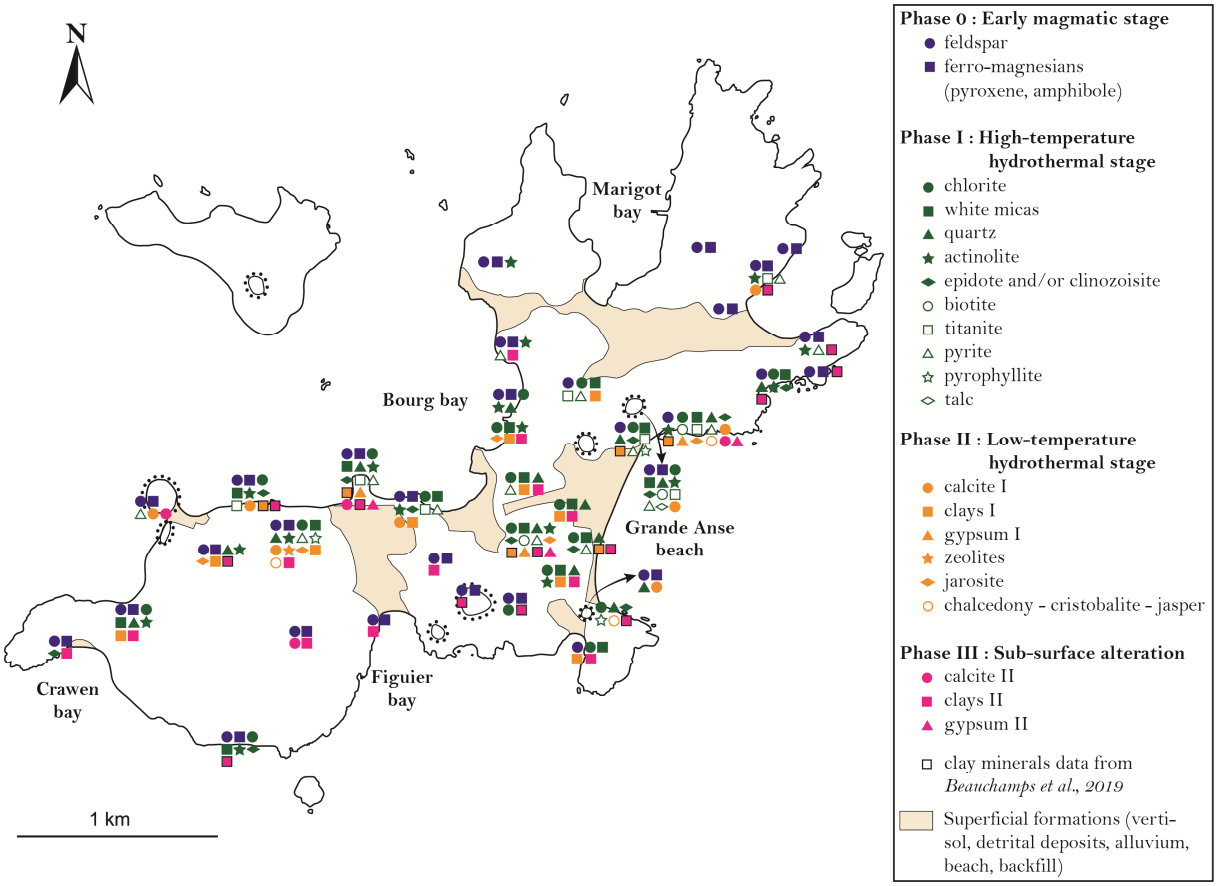

Figure 14: Distribution of different generations of mineral phases (volcanic, high and low temperature hydrothermal and sub-surface alteration) within Terre-de-Haut Island. **(COLOR / IMAGE SIZE: FULL PAGE WIDTH)**

7- P-T-XH_2O estimates for hydrothermalism

7-1- Geothermal thermometry

The mineral association (Figure 14) representative of the first hydrothermal stage is observed in multiple geothermal systems for temperatures above 300°C, while the mineralogy developed during the second hydrothermal stage is typically described for temperatures ranging between 300 and 220°C (Browne, 1978; Henley et al., 1986).

591 The late alteration stage reflects the progressive cooling history of the paleo-hydrothermal
592 system with crystallization of a sequence of minerals commonly reported for temperatures
593 below 200 °C (smectite and kaolinite, Ji and Brown, 2000; Lagat, 2014).

594 **7-2- Chlorite geothermometry**

595 Cathelineau and Nieva (1985) and Cathelineau (1988) first proposed a geothermometer
596 based on the chemical composition of chlorite. Later, more elaborated versions of this
597 thermometer have been proposed that are particularly well-adapted for hydrothermalized
598 rocks (Lanari et al., 2014; Bourdelle and Cathelineau, 2015). Following these recent
599 investigations, for Si-poor and Al-rich chlorites, the more appropriate calibration is the one
600 proposed by Lanari et al. (2014), while for Si-rich chlorites, the calibration proposed by
601 Bourdelle and Cathelineau (2015) is better adapted. We thus selected a given calibration as
602 a function of the measured chlorite chemistry.

603 Because chlorite is stable over a wide temperature range in geothermal systems (< 100°C to
604 > 350°C, Henley and Ellis, 1983; Reyes, 1990; White and Hedenquist, 1995; Lagat, 2014), it
605 is critical to distinguish the possible variations in chlorite compositions with respect to their
606 various microstructural crystallization sites. Indeed, as presented in the previous section, we
607 found the occurrence of chlorite in mineral associations representative of both the first and
608 the second hydrothermal stages.

609 To quantify the past temperature range of the Terre-de-Haut hydrothermal system, we
610 selected three samples from north of Grande Anse beach (altered rhyodacite 16STH19,
611 altered dacite 17TH16, altered andesite SA-14) in a significantly hydrothermalized domain,
612 with well-developed solution cleavage corridors. We also selected this area because it is a
613 domain without evidence of supergene alteration (Figures 2-B and 14). Moreover, in these
614 selected samples, chlorite developed in different microstructures as (1) grey automorphous
615 crystals (Figure 13-A), associated with muscovite, quartz and epidote, developed at the
616 expense of magmatic pyroxenes, and (2) green-grey to yellow fibrous grains (Figure 13-B),

associated with fibrous white micas, quartz, calcite, pyrite and/or talc, preferentially located at the rims of pseudomorphosed pyroxenes.

Interestingly, chlorite compositions evolve in relation to their microstructural position (see table 3), and even the type (I) grey automorphous grains display, in many cases, composition zoning from cores to rims. An increase in Si content and a decrease in Al content are depicted from type I automorphous to type II fibrous chlorites.

624 Table 3: Microprobe analyses and chlorite thermometry on three samples from north of Grande Anse beach: 16STH19 (altered rhyodacite),
625 17TH16 (altered dacite) and SA-14 (altered andesite). **(COLOR FOR ONLINE VERSION ONLY / IMAGE SIZE: FULL PAGE)**

Sample	**16STH19**							**17TH16**								**SA-14**			
Chlorite analysis	**grain 1**		**grain 2**		**grain 3**	**grain 4**	**grain 5**	**grain 6**			**grain 7**		**grain 8**	**grain 9**	**grain 10**	**grain 11**		**grain 12**	**grain 13**
Chlorite type	**I**	**I**	**I**	**I**	**I**	**I**	**I**	**I**	**II**	**II**	**I**	**I**	**II**	**II**	**II**	**II**	**II**	**II**	**II**
Structural position	core	rim	core	rim	core	core	core	rim	rim	rim	rim	rim	rim	rim	rim	core	rim	rim	rim
Mineral %wt																			
Al_2O_3	20,57	20,30	20,08	20,22	20,18	20,11	20,27	17,15	17,12	16,27	16,98	16,77	16,05	15,40	17,04	16,95	15,83	15,01	14,99
SiO_2	27,32	27,01	25,66	25,51	25,45	25,69	25,53	31,02	30,94	31,60	29,71	29,69	31,37	32,50	31,94	30,16	32,15	31,33	32,98
TiO_2	0,01	0,06	0,00	0,00	0,01	0,01	0,02	0,01	0,04	0,04	0,16	0,02	0,01	0,02	0,02	0,06	0,05	0,01	0,03
Na_2O	0,00	0,00	0,19	0,00	0,05	0,04	0,02	0,03	0,02	0,04	0,02	0,00	0,02	0,05	0,05	0,11	0,11	0,08	0,14
MgO	16,71	16,50	13,73	13,65	13,94	13,71	13,95	18,43	16,48	17,02	17,83	18,19	18,48	18,93	17,65	17,63	17,01	18,83	17,78
MnO	0,29	0,33	0,37	0,23	0,30	0,34	0,26	1,82	1,57	1,44	1,75	2,15	1,37	1,56	1,83	0,69	0,75	0,73	0,66
FeO	23,64	22,48	27,85	26,98	24,36	27,91	27,82	21,52	23,05	20,82	22,75	21,60	21,71	20,47	21,10	24,21	23,55	22,38	23,66
K_2O	0,00	0,00	0,00	0,00	0,00	0,00	0,00	0,01	0,02	0,08	0,02	0,01	0,02	0,02	0,02	0,04	0,04	0,01	0,05
CaO	0,09	0,10	0,00	0,00	0,00	0,00	0,00	0,28	0,37	0,46	0,28	0,20	0,33	0,31	0,44	0,18	0,76	0,23	0,57
Total	*88,63*	*86,78*	*87,88*	*86,59*	*84,29*	*87,81*	*87,87*	*90,28*	*89,60*	*87,77*	*89,50*	*88,64*	*89,36*	*89,26*	*90,09*	*90,03*	*90,26*	*88,62*	*90,87*
Structural formulae																			
Al	2,50	2,50	2,53	2,57	2,60	2,54	2,55	2,02	2,05	1,97	2,04	2,03	1,91	1,82	2,01	2,03	1,88	1,81	1,76
Al^{IV}	*1,19*	*1,17*	*1,26*	*1,25*	*1,22*	*1,26*	*1,28*	*0,76*	*0,68*	*0,54*	*0,88*	*0,89*	*0,70*	*0,55*	*0,61*	*0,87*	*0,57*	*0,69*	*0,55*
Al^{VI}	*1,31*	*1,33*	*1,27*	*1,32*	*1,38*	*1,28*	*1,27*	*1,26*	*1,37*	*1,43*	*1,16*	*1,14*	*1,21*	*1,27*	*1,40*	*1,16*	*1,31*	*1,12*	*1,21*
Si	2,81	2,83	2,74	2,75	2,78	2,74	2,72	3,11	3,14	3,24	3,03	3,05	3,17	3,27	3,19	3,06	3,24	3,20	3,29
Ti	0,00	0,01	0,00	0,00	0,00	0,00	0,00	0,00	0,00	0,00	0,01	0,00	0,00	0,00	0,00	0,00	0,00	0,00	0,00
Na	0,00	0,00	0,04	0,00	0,01	0,01	0,00	0,01	0,00	0,01	0,00	0,00	0,00	0,01	0,01	0,02	0,02	0,02	0,03
Mg	2,56	2,57	2,19	2,19	2,27	2,18	2,22	2,75	2,50	2,60	2,71	2,79	2,79	2,84	2,63	2,67	2,55	2,87	2,65
Mn	0,03	0,03	0,03	0,02	0,03	0,03	0,02	0,15	0,13	0,12	0,15	0,19	0,12	0,13	0,15	0,06	0,06	0,06	0,06
Fe	2,04	1,97	2,49	2,43	2,23	2,49	2,48	1,80	1,96	1,78	1,94	1,86	1,84	1,72	1,76	2,06	1,98	1,91	1,98
K	0,00	0,00	0,00	0,00	0,00	0,00	0,00	0,00	0,00	0,01	0,00	0,00	0,00	0,00	0,00	0,01	0,00	0,00	0,01
Ca	0,01	0,01	0,00	0,00	0,00	0,00	0,00	0,03	0,04	0,05	0,03	0,02	0,04	0,03	0,05	0,02	0,08	0,02	0,06
Total (cations)	9,94	9,92	10,02	9,97	9,92	9,99	10,00	9,88	9,83	9,79	9,93	9,93	9,87	9,82	9,81	9,93	9,83	9,91	9,83
Ox. number	*14*	*14*	*14*	*14*	*14*	*14*	*14*	*14*	*14*	*14*	*14*	*14*	*14*	*14*	*14*	*14*	*14*	*14*	*14*
Calculated temperature (°C)	**328**	**289**	**375**	**360**	**318**	**376**	**379**	**168 +/- 18**	**149 +/- 14**	**123 +/- 23**	**215 +/- 35**	**210 +/- 30**	**173 +/- 28**	**133 +/- 18**	**138 +/- 23**	**230 +/- 20**	**135 +/- 15**	**180 +/- 20**	**139 +/- 16**
	After Lanari et al., 2014							**After Bourdelle and Cathelineau, 2015**											

626 The core compositions of type I chlorites are Si-poor; thus, we used the Lanari et al. (2014)
627 calibration, which yields a temperature range of 320-380°C, with a calculated average
628 temperature, taking into account the different samples, of 355°C (standard deviation=27). For
629 the rims of type I chlorites a calculated temperature range is 180-350 °C, and the calculated
630 average temperature, considering the different samples, is 252°C (standard deviation=57).

631 Type II fibrous chlorites also have higher Si contents; in this case, as previously underlined,
632 the Bourdelle and Cathelineau (2015) calibration is the most adapted. With this calibration,
633 type (II) chlorite formed between 125 and 230°C with a calculated average temperature,
634 considering the different samples, of 140 °C (standard deviation=33).

635 Altogether, chlorite thermometers provide coherent estimations of the progressive cooling
636 registered by the various generations of chlorites developed during the two hydrothermal
637 stages. However, as frequently observed with the use of mineral chemistry-based
638 geothermometry, the calculated temperature ranges are large, mainly because of possible
639 continuous chemical exchanges between minerals during a given P-T path (Spear, 1993).
640 We therefore used thermodynamic modelling to try to improve P-T estimates for Terre-de-
641 Haut hydrothermalism.

642 **7-3- Thermodynamic modelling**

643 The intensive parameters (pressure and temperature) corresponding to the high-temperature
644 hydrothermal stage were calculated with the free energy minimization program THERIAK-
645 DOMINO (De Capitani and Petrakakis, 2010, updated software v. 4 February 2017) and the
646 internally consistent thermodynamic "tcdb55c2d" database (Holland and Powell, 2004).
647 Mixing models used for solid solutions are presented in the appendix (table A-5). This
648 approach is a powerfull tool to quantify the P-T-XH_2O conditions for hydrothermalism.
649 Considering the goal of this paper, we used thermodynamic modelling instead of reactive
650 transport modelling, the latter being more oriented on quantification of fluid-rock reaction for
651 a specific surface area and thus calculation of reaction rates.

To be as close as possible to the equilibrium conditions at the scale of the whole rock, which is essential for the application of this type of method, we selected a highly transformed rhyodacite (16STH19) with a maximum of secondary phases expressed.

P-T pseudosections were calculated in the SiO_2-Al_2O_3-TiO_2-FeO-MnO-MgO-CaO-Na_2O-K_2O-H_2O system using the whole rock composition of the selected sample (table 4). The observed mineral assemblage involves albite + chlorite + muscovite + biotite + clinozoisite + epidote s.s. + quartz. Under tropical conditions, the iron oxidation state is always difficult to estimate. To test the effect of Fe_2O_3 in our models, we calculated pseudosections with various amounts of Fe^{3+}. When the latter reaches 5%, we never find the mineral assemblage observed in the natural sample. Consequently, we believe a model with total iron considered FeO is the best approximation for pseudosection calculations.

Table 4: Whole-rock composition of 16STH19 sample and corresponding input in Theriak-Domino program. **(COLOR FOR ONLINE VERSION ONLY / IMAGE SIZE: COLUMN WIDTH)**

Sample 16STH19				
Composition (%)			**Input Theriak-Domino (mol)**	
SiO_2		59.555	**Si**	50.489
Al_2O_3		16,070	**Al**	16.058
Fe_2O_3		1.772	**Fe**	1.129
MnO		0.103	**Mn**	0.074
MgO		3.055	**Mg**	3.862
CaO		5.531	**Ca**	5.024
Na_2O		1.691	**Na**	2.780
K_2O		1.299	**K**	1.405
TiO_2		0.558	**Ti**	0.365
P_2O_5		0.151	**P**	0.109
LOI		10.214	**H**	57.761
26.46 %	*$CO_{2\ total}$*	*2.703*	**O**	?
58.97 %	*H_2O_{total}*	*6.023*		
7.04 %	*FeO*	*0.719*		
7.53 %	*S_{total}*	*0.769*		

668 We considered the fluid phase in excess to be consistent with the conditions of a fluid-
669 saturated hydrothermal system. However, in high-temperature geothermal systems, fluids
670 have different origins (meteoric waters with or without sea-water components, volcanic fluids
671 and gases with variable amounts of CO_2, H_2S or SO_2); thus, it seems critical to test the effect
672 of fluid composition on the modelled system. In the first approach, a pseudosection was
673 calculated with 100% H_2O for the fluid composition. In this case, the observed mineral
674 assemblage corresponds to the calculated field (360-375°C and 0.90-1.40 kbar) identified
675 with bold-black characters in figure 15-A and is in agreement with the highest temperature
676 values obtained by chlorite geothermometry on type-1 chlorite cores from this sample
677 (16STH19, see figure 15-B and table 4). This stability field is indeed limited by the
678 appearance of wairakite and the disappearance of clinozoisite towards low temperatures and
679 pressures. A temperature of approximately 365°C is an estimation consistent with both
680 methods. In a second test, a specific P-XH_2O pseudosection (with XH_2O representing the
681 variability of amount of water, in moles, in the considered system) was calculated to decipher
682 the effect of the amount of H_2O in the fluid present in excess on the pressure estimates
683 (Figure 15-C). The observed mineral assemblage is stable for a large range of XH_2O values,
684 i.e., between 12% and 100%. The chemical components of the LOI (see table 3) allows an
685 estimation of the components in the fluid phase with respect to the bulk-rock chemistry of the
686 analysed sample. In the 16STH19 sample, the amount of H_2O in the fluid phase is estimated
687 at approximately 59%, with a CO_2 content of approximately 27%. The result of our
688 thermodynamic modelling is completely consistent with this estimation and indicates that
689 regardless of the XH_2O value, as long as is greater than 12%, the observed mineral
690 assemblage remains stable. Consequently, in the studied sample, for the XH_2O values of
691 interest and for a temperature of approximately 365°C, the modelled pressure range is
692 restricted to between 0.95 and 1.15 kbar.

693 The results obtained from various hydrothermal and/or geothermal fields demonstrate that an
694 increase in the CO_2 concentration in the hydrothermal fluid would have displaced the

695 equilibrium into the calcite-stable field at the expense of epidote and/or wairakite stability
696 (Browne and Ellis, 1970; Hedenquist, 1986; Hedenquist and Browne, 1989; Browne, 2003).
697 In our model, the addition of CO_2, which is present in our system as previously underlined,
698 shifts the wairakite stability towards lower temperatures, on the order of approximately fifteen
699 degrees, and pressures, on the order of approximately 0.05 kbar. Therefore, the best P-T
700 estimate for the highest temperature stage of hydrothermalism corresponds to a temperature
701 of approximately 350°C for a pressure between 0.9 and 1.1 kbar.

702

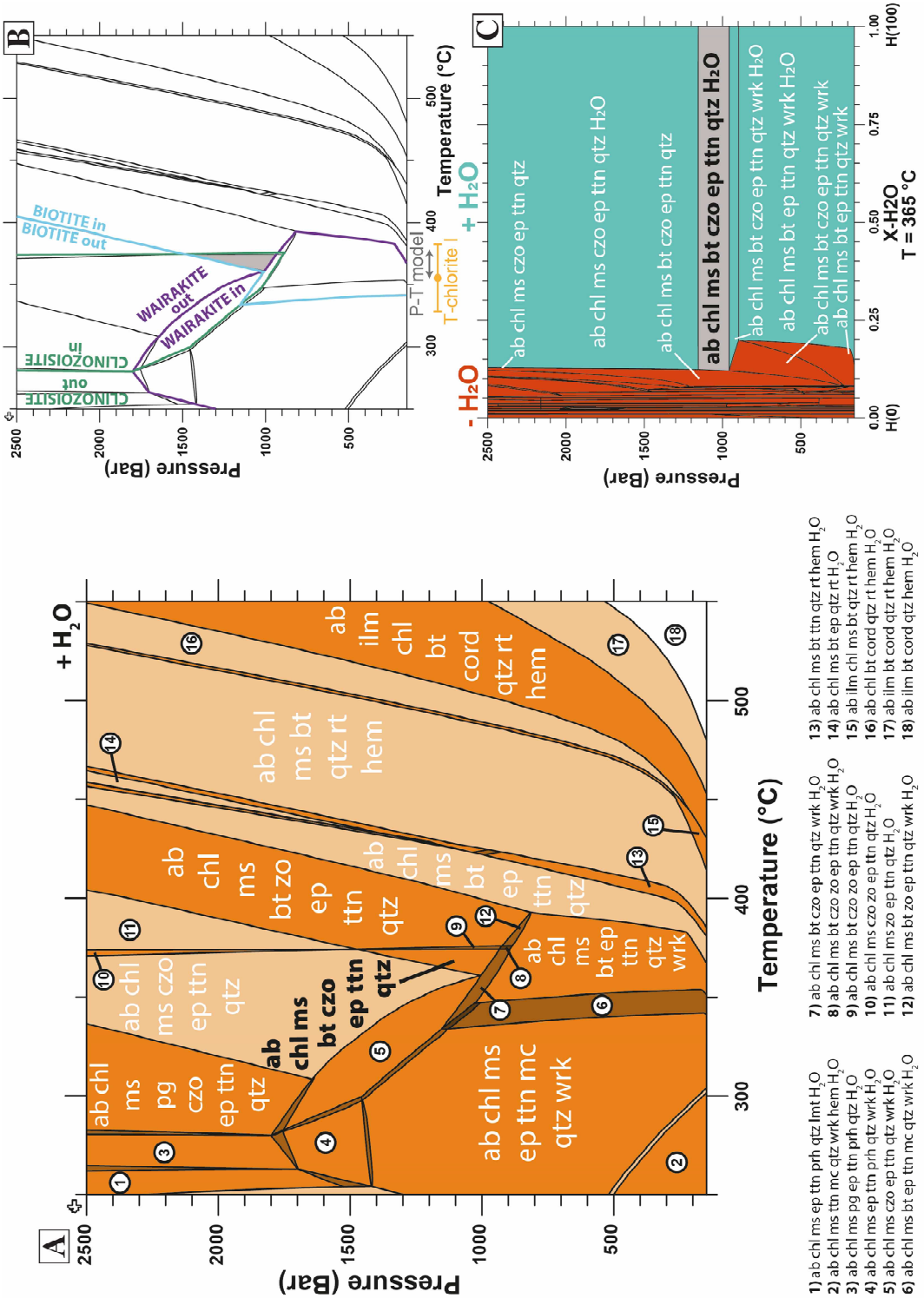

Figure 15: A) Calculated P-T pseudosection for a rhyodacite sample (16STH19) with H_2O saturation and total iron as Fe^{2+} with Theriak-Domino program (De Capitani and Petrakakis, 2010, updated software v. 4 February 2017) and "tcdb55c2d" database (Holland and Powell, 2004). Rock composition is in mol.% oxide. Fields are coloured with according to their variances, darker colours indicating higher-variance assemblages. The stability field written in bold correspond to the observed assemblage. B) Simplified representation of the P-T pseudosection with the stability field of the observed mineral association in grey. C) P-X(H_2O) equilibrium phase diagram calculated at 365°C, with similar composition in Figure 15-A, and modelled between 0 (H = 0) and 100 moles (H = 100). The field coloured in grey corresponds to the observed assemblage. Mineral abbreviations are from Kretz, 1983. **(COLOR / IMAGE SIZE: FULL PAGE WIDTH)**

8- Discussion

8-1- Relationship between deformation and hydrothermalism: implications for fluid transfer pathways

In a general cross-section of Terre-de-Haut Island, the main altered zone is localized within a WNW-ESE graben (Figure 16-A). However, we discovered the occurrence of ductile tectonic structures, precisely pressure solution cleavages concentrated in specific shear zones, clearly intersected, and thus overprinted, by numerous brittle faults (Figure 16-A). Moreover, we established that the crystallization of the high-temperature hydrothermal phases (i.e., the first stage of hydrothermal alteration) is contemporaneous with the development of ductile tectonic structures. At the regional scale, this is highlighted by the comparison between the structural and mineralogical maps (Figures 7 and 14). Our microstructural observations indicate that a stress-induced pressure solution process is the mechanism leading the development of ductile tectonic structures. Numerous studies have shown that pressure solution creep involves grain dissolution in the zones of highest stress, mass transfer of the most soluble chemical elements away from dissolution sites in a free-fluid phase, and deposition of these elements in the zones of smallest stress (veins, micro-cracks, pores, etc.; Sorby, 1863; Ramsay, 1967; Rutter, 1972, 1976; Siddans, 1972; Elliot, 1973; Kerrich, 1977; Beach, 1979). This implies fluid circulation in the open spaces (pores and cleavages) of the rocks located in the ductile corridors. Similar structural pathways for fluid transfers are well documented in various cases of actively deforming ductile crust (Mc Caig, 1988; Oliver, 1996; Famin et al., 2004; Mulch et al., 2006).

In the study area, fluids necessarily react with volcanic minerals to produce the observed high-temperature secondary phases. Indeed, to be produced, the observed microstructure requires:

(1) H2O-rich fluid infiltration in the volcanic rock, stress-induced dissolution of anorthoclase microlites and, to a lesser extent, some phenocryst rims, leaving space for concentration of insoluble minerals;

742 (2) transfer of at least K, Si, Al and Na in the free fluid film in the pore space of the rock;
743 (3) reaction of pyroxenes with a part of this fluid phase trapped at phenocryst contacts and
744 crystallization of micas, chlorite, albite and quartz at the expense of pyroxenes;
745 (4) expulsion of the fluid phase in excess through pores and/or micro-cracks and veins.

746 In such a case, the ductile corridors are not sites of fluid production but only pathways for
747 fluid transfer. However, progressive mineral crystallization tends to close spaces, and a given
748 shear zone can be sealed by secondary phases (Navelot et al., 2018). Because the whole
749 process implies different steps, i.e., dissolution, transfer and crystallization, if the rate of a
750 given step is slower than the others, it will control the kinetics of the whole process and thus
751 control the fluid circulation. Therefore, a structure being a fluid pathway at a given increment
752 of hydrothermal system development can act as a barrier to fluid transfer later. In this case,
753 there must be relays between the transfer zones to maintain the activity of the hydrothermal
754 system. In dealing with this issue, the geometry of the finite strain pattern is a crucial
755 element. In the area of interest, ductile shear zones with different dips tend to anastomose
756 (sector 1 in Figure 7-A, east of Fond Curé in Figure 16-A), and in other cases (sector 2 in
757 Figure 7-A, west of Morne Rouge in Figure 16-A), subvertical ductile corridors clearly
758 intersect other moderately dipping zones. If connected, the geometric relays between
759 anastomosed shear zones with contrasted dips are particularly favourable to both vertical
760 and lateral fluid transfers, while the intersections between superposed ductile corridors allow
761 the persistence of fluid transfer through time to be envisaged.

762

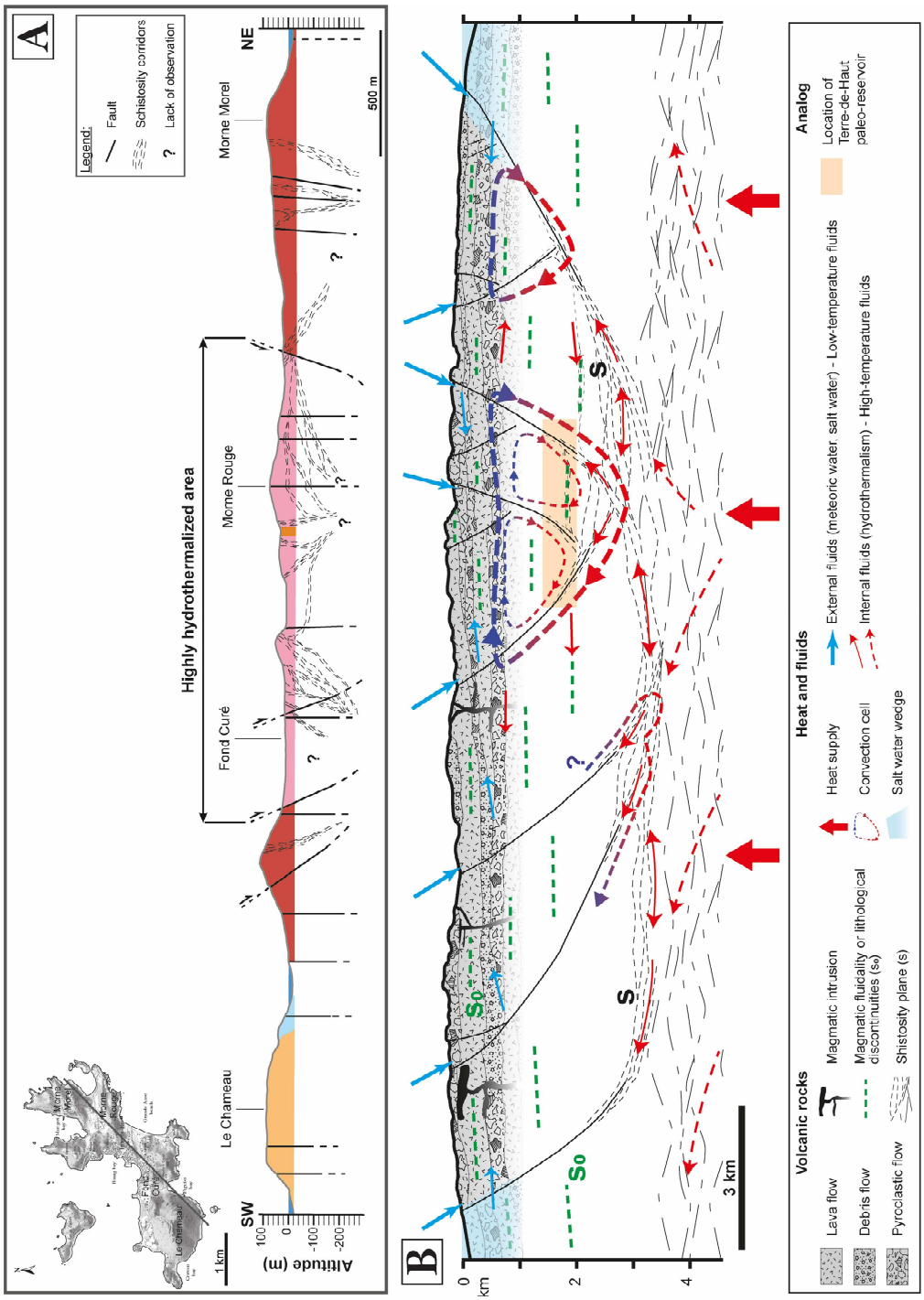

763

764 Figure 16: A) NE-SW cross-section from Terre-de-Haut Island displaying the superposition of
765 brittle faults upon the network of schistosity planes. The highly hydrothermalized area is
766 located in the central part of the cross-section within a WNW-ESE graben. The colours are
767 similar to the ones of the geological map in figure 2-B (localisation of the cross-section). B)
768 Conceptual model of the geothermal reservoir in the Guadeloupe magmatic island arc. This
769 north-south cross section displays the possible plumbing system of the geothermal reservoir,
770 from the surface to the deeper parts, with the different fluid flow contributions. The
771 brittle/ductile transition is represented as a sub-horizontal horizon acting as a crustal scale
772 shear zone. The geometry of faults and schistose zones pattern is purely indicative. The
773 geological formations are only illustrated schematically over the first kilometre of the cross-
774 section. **(COLOR / IMAGE SIZE: FULL PAGE WIDTH)**

During the exhumation and thus the thermal evolution (i.e., cooling) of the paleo-hydrothermal system, low-temperature hydrothermal phases continue to crystallize in fractures, veins and brittle faults, as well as in some shear zones. Indeed, if some veins are contemporaneous with the solution cleavage formation and indicate incremental extension parallel to the planar structures, late veins and fractures are related to a second and independent deformation episode under brittle conditions. This recent to active brittle extension is well documented in the area of interest (Feuillet et al., 2001, 2002, 2004; Bazin et al., 2010; Leclerc et al., 2016; Verati et al., 2016; Navelot et al., 2018). These late tectonic structures contain, or are underlined by, supergene clay minerals (illite, smectite) or zeolites. This means that during the cooling history of the hydrothermal system, tectonic structures continue to be preferential drains, allowing the circulation of fluids. These observations are consistent with different works indicating that in tectonically active regions, such as the Guadeloupe archipelago, earthquake faulting is possibly associated with seismic pumping, a process that can enhance channelized fluid flow and thus fluid migration from production zones towards open spaces, i.e., dilatation zones (Sibson et al., 1975; Garven and Raffensperger, 1997; Famin et al., 2005).

8-2- The paleo-depth of the Terre-de-Haut exhumed hydrothermal system

Pressure is a crucial parameter that must be quantified to constrain the dynamics of geological systems. Thermodynamic laws applied to mineralogy are powerful tools to address this question, and pressure quantification is constrained by the stability fields of specific mineral assemblages (Spear, 1993; Bucher and Frey, 2002, with references therein). In such a case, and by definition, the calculated pressure, often called “thermodynamic pressure” (Kondepudi and Pigogine, 1998), is an intensive parameter independent of the physical parameters that control the “effective pressure” applied to a given rock (Fermi, 1936; Korzhinskii, 1965). In crustal rocks, within which both solid and fluid phases are present, both hydrostatic and lithostatic pressure must be considered physical components of the effective pressure (Jaeger, 1969; Fyfe et al., 1978; Jaeger and Cook, 1979; Yardley, 2009; Moulas et

al., 2019). In the uppermost part of the crust (first few kilometres), as observed in boreholes located worldwide, there are enough fractures, veins and open connected pores that the free fluid phase within these voids is under hydrostatic pressure. With increasing depth (between 2 and 3 km), the interconnected networks of pores and fractures tend to close, and the pore pressure increases and tends to approach lithostatic pressure (Coyle and Zoback, 1988; Ehrenberg, 1993; Buller et al., 2005; Nadeau and Ehrenberg, 2006; Taylor et al., 2010; Nadeau, 2011; Sachau et al., 2015).

In shallow crustal hydrothermal systems, as in geothermal systems, both hydrostatic and lithostatic pressures are physical parameters that control the effective pressure (Nor and Walder, 1992; van Ruth and Hillis, 2000; Rowland and Simmons, 2012; Sachau et al., 2015; Chambefort et al., 2017). Pore pressure acts against minerals in the opposite sense of lithostatic pressure, and consequently, the effective pressure is lithostatic pressure reduced by hydrostatic pressure (Batchelor, 1967),

To restore the paleodepth of the Terre-de-Haut paleohydrothermal system, we have to consider a lithostatic gradient calculated with a mean dry bulk density adapted to the lithology of a volcanic arc (basaltic andesites, andesites, dacites and rhyodacites) that is approximately 2.6 $kg/m^3 \cdot 10^{-3}$ (Klein and Johnson, 1983). Thus, the lithostatic gradient increases by 26 MPa/km. Because, in volcanic arcs, and particularly in the case of the Guadeloupe arc, fluids in hydrothermal and geothermal systems are dominated by H_2O, the hydrostatic gradient must be approximately 10 MPa/km. Consequently, in the uppermost part of the arc crust, $P_{fluid} \approx 1/2.6\ P_{lithostatic}$ and effective pressures in the case of interest range between 0.55 and 0.68 kbar. This was the case for the Terre-de Haut paleo-reservoir 3 or 2 Ma ago (i.e., during island volcanic activity, Zami et al., 2014), at depth between 1.4 and 1.8 km. The timescale for exhumation of this paleo-reservoir is therefore consistent with erosion rates proposed for the Guadeloupe archipelago (Sak et al., 2010; Lloret et al., 2011; Rad et al., 2013; Ricci et al., 2015a, b).

8-3- A conceptual scheme for high-energy geothermal systems in the Guadeloupe archipelago

8-3-1- The uppermost boundary of the conceptual scheme

To constrain the uppermost part of our scheme (Figure 16-B), we have a large number of published surface data, some of which was obtained in the active geothermal system of Bouillante and some was obtained in the last five years on Terre-de-Haut Island.

We want to stress that an important result of the last two decades of tectonic and geophysical research is the fact that the tectonic pattern of the whole Guadeloupe archipelago results, since the last 5 Ma, from arc-parallel extension combined with transcurrent faults (i.e., transtensional regime, Julien and Bonneton, 1989; Feuillet et al., 2002, 2004, 2010; Mathieu et al., 2011; Laigle et al., 2013; Münch et al., 2013; De Min et al., 2015; Leclerc et al., 2016). In this tectonic framework, the Bouillante active geothermal system is located in a “horsts and grabens” system bounded by E-W oriented normal faults associated with a N160 oriented transcurrent fault (Bouchot et al., 2010, 2014; Thinon et al., 2010; Calcagno et al., 2012, and Figure 1-C). Numerous investigations have established that (1) brittle faults contribute to fluid flow through the recharge of the system in supergene fluids (dominant meteoric water and minor seawater, Bouchot et al., 2010; Millot et al., 2010; Sanjuan et al., 2010), (2) vertical clay mineral zonation, typical of hydrothermally altered systems and utilized in geothermal fields worldwide, is well developed along the available boreholes (Mas et al., 2006) and (3) temperatures in the range of 230-255°C are measured at depths between 475 m and 1.2 km (Guillou-Frottier, 2003; Bouchot et al., 2010; Mas et al., 2006; Sanjuan et al., 2001, 2004).

In our previous works on Terre-de-Haut Island, we provide datasets on brittle fault geometry and kinematics as well as on thermo-physical properties of hydrothermalized rocks (Verati et al., 2016; Navelot, 2018; Navelot et al., 2018; Favier, 2019). We observed, here also, that fault intersections are suitable for fluid transfers, particularly when the faults are connected to

fractured lavas or cooling joints in lavas. In this case, the intersections between highly dipping faults or fractures and sub-horizontal volcanic structures are favourable geometries for both vertical and lateral fluid transfers.

8-3-2- The lowermost boundary of the conceptual scheme

In the Guadeloupe archipelago, a recent study (Manga et al., 2012) revealed a steady-state conductive gradient between 69.3 ± 1.5 and 98.2 ± 8.8 °C/km. As demonstrated by mineralogical and petrological investigations on the oldest, and thus most eroded, volcanic units of the considered archipelago, this conductive gradient did not change during the last 5 Ma (Verati et al., 2018; Favier, 2019; Favier et al., 2019). Similar thermal conditions are well known and generalized in numerous examples of recent and active as well as old and exhumed magmatic arcs located on the upper plates of subduction zones (Miyashiro, 1961; McKenzie and Sclater, 1968; Hasebe et al., 1970; Oxburgh and Turcotte, 1970; Watanabe et al., 1970; Ernst, 1971; Sclater, 1972; Furukawa and Uyeda, 1989; Ribe, 1989; Cloos, 1993; Furukawa et al., 1998; Fukahata and Matsu'ura, 2000; England and Wilkins, 2004; Ranalli and Rybach, 2005). In the area of interest, temperatures close to or higher than 300°C are thus reached at depths between 4 and 5 km, and consequently, since 5 Ma, the brittle-ductile transition is necessarily localized at that depth in the arc crust. This shallow depth rheological horizon constitutes the lowermost boundary of our conceptual scheme (Figure 16-B), and its position is consistent with the thermomechanical conditions recognized in subduction zones' upper plates, for example, in the Mediterranean region, in the Tuscany magmatic province in Italy, where the Larderello geothermal field is located (Batini et al., 1983; Cameli et al., 1998; Liotta and Ranalli, 1999; Bellani et al., 2004; Bertini et al., 2006; Liotta and Brogi, 2020), or in Anatolia (Menderes Massif), which is also recognized as an active geothermal domain even in a different arc setting (Aydin et al., 2005 ; Erkan, 2015; Roche et al., 2018). In the thermomechanical framework of a magmatic arc, it is thus necessary to consider that the steeply dipping brittle faults, well developed in the uppermost part of the arc crust, will

become more horizontal and will progressively root on the frictional-viscous boundary (Hobbs et al., 1976; Jaeger et al., 2009; Nicolas and Poirier, 1976; Kirby, 1983).

8-3-3- Terre-de-Haut hydrothermal system in the conceptual scheme: an analogue of geothermal systems' roots in magmatic arcs

The paleo-depth of the Terre-de-Haut exhumed hydrothermal system was estimated to be between 1.4 and 1.8 km. At these depths, the occurrence of hydrothermal mineral assemblages that are stable under a temperature of approximately 350 °C suggests a significant thermal anomaly with respect to the regional standard geothermal gradient. This paleotemperature is even higher than the temperatures proposed for the active Bouillante field (Mas et al., 2006) but is compatible with downhole temperature ranges in different geothermal fields around the world (Browne, 1978; Moro et al., 1982; Bertini et al., 1991; Battaglia et al., 1991; White and Hedenquist, 1995; Bogie et al., 2008; Bouchot and Genter, 2009; Bertani et al., 2018; Cherkose and Mizunaga, 2018). Furthermore, in the area of intensely altered rocks located in the WNW-ESE graben, the primary volcanic mineral assemblages are frequently replaced beyond recognition. Indeed, the anhydrous minerals of the volcanic rocks (mainly pyroxenes, plagioclases and anorthoclases) are replaced by hydrated phases (white micas, chlorites, biotites, pyrophyllites, etc.) until the formation of clay minerals at the end of the alteration process. Such a mineralogical evolution requires significant H_2O-rich fluid infiltrations in the volcanic rocks during the progressive exhumation, and thus cooling, of the paleo-hydrothermal system. Additionally, high-temperature hydrothermal fluid circulation was effective enough during the first stages of the alteration history to frequently erase the primary volcanic structures and to allow tectonic structures (i.e., ductile shear zones), driven by stress-induced pressure solution processes, to be developed.

When taken together, these observations lead us to consider that the Terre-de-Haut hydrothermal system represents a piece of arc crust that was located, 2 or 3 Ma ago, at a depth of 1.5-2 km, and submitted to a significant thermal anomaly and to important fluid

907 percolations. This system offers the opportunity to characterize the transfer structure of
908 hydrothermal fluids in a position equivalent to the root of the geothermal systems in the
909 Lesser Antilles magmatic arc. In this area of interest, we discovered the occurrence of ductile
910 shear zones generated by pressure solution processes coeval with the development of high-
911 temperature hydrothermal mineral associations at the expense of primary volcanic phases.
912 This demonstrates that, at shallow crustal depths under fluids' present conditions, pressure
913 solution creep interacts and is in competition with brittle deformation, as established in the
914 last forty years by natural observations and experimental or theoretical modelling (Rutter,
915 1983; Renard et al., 2000; Dysthe et al., 2002, 2003; Sibson and Rowland, 2003; Gratier et
916 al., 2009, 2013). Therefore, stress-driven fluid and mass transfer creep laws accommodate
917 ductile shear zones development in the upper arc crust. In Terre de Haut Island, the
918 observed shear zones must be considered pathways for fluid infiltration, and because they
919 have variable dips, they constitute a structure favourable for both vertical and lateral fluid
920 transfers. They also represent the geometric connection between the near-surface brittle
921 faults and the brittle-ductile, sub-horizontal, transition horizon.

922 In the proposed conceptual scheme of a magmatic arc evolving under an extensional
923 tectonic regime, the abnormal heat flow is the result of arc-related magmatism, which
924 transfers differentiated magmatic melts, heat and high temperature fluids towards the upper
925 crustal levels. In this context of the supra-subduction zone, magmatic sources can be
926 envisaged for volatile components. These deep, hot fluids can be channelized and/or trapped
927 in the brittle-ductile transition horizon and expulsed in the more permeable sectors of this
928 horizon.

929 In the uppermost part of our scheme (Figure 16-B), as demonstrated by numerous
930 investigations in the active Bouillante geothermal system, the downward flow of supergene
931 cold fluids is efficient along conjugated normal faults (Figure 1-C), which act as preferential
932 strongly dipping pathways (Sanjuan and Brach, 1997; Guillou-Frottier, 2003; Bouchot and
933 Genter, 2009; Lachassagne et al., 2009; Bouchot et al., 2010; Thinon et al., 2010; Calcagno

et al., 2012). Lithological contacts and volcanic structures can also account for lateral movements of fluids (Navelot et al., 2018). Between the first kilometre of arc crust and the brittle-ductile transition horizon, the extensional shear zones observed in the Terre-de-Haut analogue act as transfer zones where circulation of geothermal fluids is possible. The geometry of the finite shear zone pattern suggests that geothermal fluids can be vertically or laterally channelled and/or stored in tectonic structures.

Finally, in the proposed conceptual scheme (Figure 16-B), the shear zones, driven by stress-induced pressure solution processes, may have an important enhancing role in establishing an advective regime in the whole geothermal system.

Addressing deep geothermal exploration, our investigations suggest that in magmatic arcs:

- Ductile tectonic structures are efficient pathways for geothermal fluid flows, as already proposed by other authors (Baldi et al., 1995; Liotta and Ranalli, 1999; Brogi et al., 2003, 2005; Bellani et al., 2004; Kaya, 2015; Roche et al., 2018; Liotta and Brogi, 2020),

- Tectonic and volcanic structures contribute to fluid flows and could be efficient drains for both vertical and lateral fluid circulations and/or storage,

- The brittle-ductile transition horizon, located at shallow depths, could act as a permeable zone where the transfer of deep geothermal fluids is facilitated. It may potentially be considered a deep-seated reservoir hosting an important geothermal resource.

9- Conclusions

We document and describe, for the first time in Terre-de-Haut Island (Les Saintes volcanic archipelago), the occurrence of ductile deformation, i.e., shear zones generated by pressure solution processes coeval with the development of high-temperature hydrothermal mineral associations.

(1) Using conventional thermometry and thermodynamic modelling, we demonstrate that the hydrothermal system of Terre-de-Haut Island developed at a temperature of approximately 350°C and at depths in the range of 1.4 – 1.8 kilometres.

(2) The link between mineral transformations and ductile deformation suggests first that shear zones are efficient pathways for geothermal fluid flows and second that both vertical and lateral fluid transfers are possible in the crust of the Lesser Antilles volcanic arc.

(3) Together with preceding available structural, mineralogical and petrophysical data, this study clearly establishes that the highly hydrothermalized area of Terre-de-Haut Island corresponds to an eroded and exhumed geothermal paleo-reservoir. It is thus a key analogue for understanding the roots of current active geothermal systems in supra-subduction volcanic arcs.

10- Acknowledgements

This paper is a contribution to the GEOTREF program, funded by French government (program “Investissements d’Avenir” tutored by ADEME). We thank the researchers from the GEOTREF consortium for discussions during the fieldwork campaigns and scientific meetings. The authors thank Gabriel Monge (CEMEF laboratory) for the use of the X-ray Diffraction device.

We sincerely would like to thank the reviews, the comments and the suggestions of Isabelle Chambefort and of an anonymous reviewer that significantly improved the manuscript. The authors thank José Luis Macías for useful editorial work.

11- Appendices

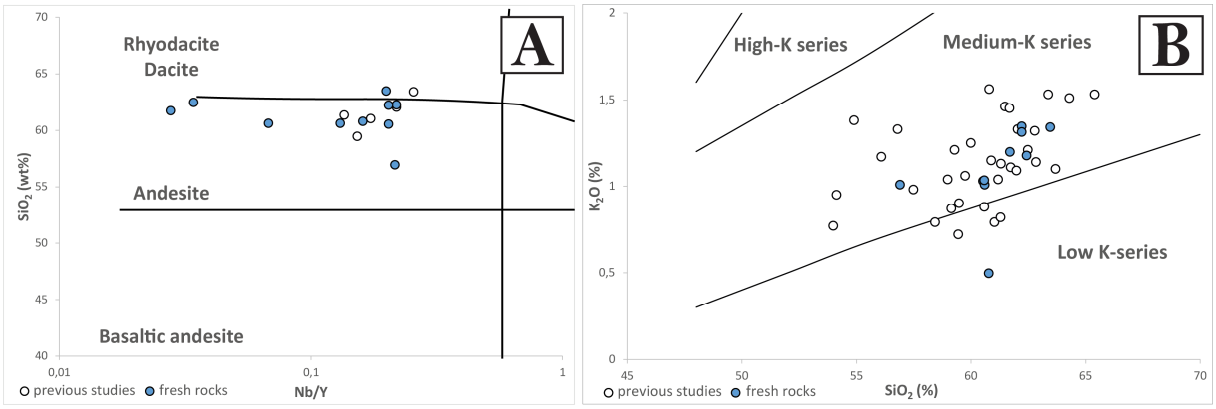

Figure A-1: A) SiO_2 vs. Nb/Y diagram after Winchester and Floyd 1977, white circles represent previous data from Jacques and Maury, 1988; Zami et al., 2014 and Navelot et al., 2018. Blue circles correspond to our new analyses. B) SiO_2 vs. K_2O plot after Peccerillo and Taylor (1976), white circles represent previous data from Jacques et al., 1984; Jacques and Maury, 1988; Zami et al., 2014 and Navelot et al., 2018. Blue circles correspond to our new analyses.

Table A-1: Table of whole rock major and trace element analyses. Total major element analyses not recalculated to 100%.

Excel file

Table A-2: Electron microprobe analyses and structural formula of volcanic phases

Excel file

Table A-3: Electron microprobe analyses of low-temperature hydrothermal phases

Excel file

Table A-4: Electron microprobe analyses and structural formula of high-temperature hydrothermal phases

Excel file

Table A-5: Table of mixing models solid solution used in tcdb55c2d database of Theriak-Domino software

Excel file

12- References

ABOU-AKAR, A., MATRAY, J.-M., & BRACH, M. 1992. Etude Géochimique Du Fluide Géothermal Du Puits BO2 (Central EDF) et Des Sources Thermales de La Région de Bouillante (Guadeloupe), Report BRGM-R-36203 IRG SGN 92. Orléans.

AYDIN, İ., KARAT, H.İ., & KOÇAK, A. 2005. Curie-point depth map of Turkey. Geophysical Journal International, 162, 633–640, doi: 10.1111/j.1365-246X.2005.02617.x.

BAIRD, A.F., KENDALL, J.-M., SPARKS, R.S.J., & BAPTIE, B. 2015. Transtensional deformation of Montserrat revealed by shear wave splitting. Earth and Planetary Science Letters, 425, 179–186, doi: 10.1016/j.epsl.2015.06.006.

BALDI, P., BELLANI, S., CECCARELLI, A., FIORDELISI, A., SQUARCI, P., & TAFFI, L. 1995. Geothermal anomalies and structural features of southern Tuscany. In: World Geothermal Congress Proceedings, Florence. Florence, 1287–2391.

BAS, M.J.L., MAITRE, R.W.L., STRECKEISEN, A., & ZANETTIN, B. 1986. A Chemical Classification of Volcanic Rocks Based on the Total Alkali-Silica Diagram. Journal of Petrology, 27, 745–750, doi: 10.1093/petrology/27.3.745.

BATCHELOR, G.K. 1967. An Introduction to Fluid Dynamics. London, Cambridge University Press.

BATINI, F., BERTINI, G., GIANELLI, G., PANDELI, E., & PUXEDDU, M. 1983. Deep structure of the Larderello field: contribution from recent geophysical and geological data. Soc. Geol. Ital. Mem., 25, 219–235.

BATINI, F., BROGI, A., LAZZAROTTO, A., LIOTTA, D., & PANDELI, E. 2003. Geological features of Larderello-Travale and Mt. Amiata geothermal areas (southern Tuscany, Italy). Episodes, 26, 239–244.

BATTAGLIA, S., GIANELLI, G., ROSSI, R., & CAVARRETTA, G. 1991. The sulphur springs geothermal field, St. Lucia, lesser Antilles: Hydrothermal mineralogy of wells SL-1 and SL-2. Journal of South American Earth Sciences, 4, 1–12, doi: 10.1016/0895-9811(91)90014-C.

1038 BAU, M. 1991. Rare-earth element mobility during hydrothermal and metamorphic fluid-rock
1039 interaction and signifiance of the oxidation state of europium. Chemical Geology, 93, 219–
1040 230, doi: 10.1016/0009-2541(91)90115-8.
1041 BAZIN, S., FEUILLET, N., DUCLOS, C., CRAWFORD, W., NERCESSIAN, A.,
1042 BENGOUBOU-VALÉRIUS, M., BEAUDUCEL, F., & SINGH, S.C. 2010. The 2004–2005 Les
1043 Saintes (French West Indies) seismic aftershock sequence observed with ocean bottom
1044 seismometers. Tectonophysics, 489, 91–103, doi: 10.1016/j.tecto.2010.04.005.
1045 BEACH, A. 1979. Pressure solution as a metamorphic process in deformed terrigenous
1046 sedimentary rocks. Lithos, 12, 51–58, doi: 10.1016/0024-4937(79)90062-8.
1047 BEAUCHAMPS, G., LEDÉSERT, B., HÉBERT, R., NAVELOT, V., & FAVIER, A. 2019. The
1048 characterisation of an exhumed high - temperature paleo - geothermal system on Terre - de -
1049 Haut Island (the Les Saintes archipelago , Guadeloupe) in terms of clay minerals and
1050 petrophysics. Geothermal Energy, 1–18, doi: 10.1186/s40517-019-0122-y.
1051 BECK, R.H. & LEHNER, P. 1974. Oceans, New Frontier in Exploration. The American
1052 Association of Petroleum Geologists Bulletin, 58, 376–395.
1053 BELLANI, S., BROGI, A., LAZZAROTTO, D., LIOTTA, D., & RANALLI, G. 2004. Heat flow,
1054 deep temperatures and extensional structures in the Larderello Geothermal Field (Italy) :
1055 constraints on geothermal fluid flow. Journal of Volcanology and Geothermal Research, 132,
1056 15–29, doi: 10.1016/S0377-0273(03)00418-9.
1057 BERTANI, R., BÜSING, H., BUSKE, S., DINI, A., HJELSTUEN, M., LUCHINI1, M.,
1058 MANZELLA, A., NYBO, R., RABBEL, W., SERNIOTTI, L., & THE DESCRAMBLE SCIENCE
1059 AND TECHNOLOGY TEAM. 2018. The First Results of the DESCRAMBLE Project. In:
1060 PROCEEDINGS, 43rd Workshop on Geothermal Reservoir Engineering. Stanford University,
1061 Stanford, California, February 12-14, 2018, 16.
1062 BERTINI, G., CAMELI, G.M., COSTANTINI, A., DECANDIA, F.A., DI FILIPPO, M., DINI, I.,
1063 ELTER, F.M., LAZZAROTTO, A., LIOTTA, D., PANDELI, E., SANDRELLI, F., & TORO, B.
1064 1991. Struttura geologica fra i monti di Campiglia e Rapolano Terme (Toscana meridionale):

1065 stato attuale delle conoscenze e problematiche. Studi Geologici Camerti, volume speciale,
1066 155–178.
1067 BERTINI, G., CASINI, M., GIANELLI, G., & PANDELI, E. 2006. Geological structure of a
1068 long-living geothermal system, Larderello, Italy. Terra Nova, 18, 163–169, doi:
1069 10.1111/j.1365-3121.2006.00676.x.
1070 BLANC, F. 1983. Corrélations Chronologiques et Géochimiques Des Formations
1071 Volcaniques Du Sud de La Basse-Terre de Guadeloupe (Petites Antilles) : Début Du Cycle
1072 Récent. Université Scientifique et Médicale de Grenoble, Grenoble.
1073 BOGIE, I., KUSUMAH, Y.I., & WISNANDARY, M.C. 2008. Overview of the Wayang Windu
1074 geothermal field, West Java, Indonesia. Geothermics, 37, 347–365, doi:
1075 10.1016/j.geothermics.2008.03.004.
1076 BORRADAILE, G. J., BAYLY, M. B., & POWELL, C. 1982. Atlas of Deformational and
1077 Metamorphic Rock Fabrics. Borradaile, Graham J., Bayly, M. Brian & Powell, C. M. (eds).
1078 Berlin, Heidelberg, Springer Berlin Heidelberg, doi: 10.1007/978-3-642-68432-6.
1079 BOUCHOT, V. & GENTER, A. 2009. Exploration guides for active high-temperature
1080 geothermal systems as modern analogs for epithermal paleosystems. In: Geothermal
1081 Resources Council 2009 Annual Meeting October 4-7 2009, Reno, Nevada, USA. Reno,
1082 Nevada, USA.
1083 BOUCHOT, V., TRAINEAU, H., GUILLOU-FROTTIER, L., THINON, I., BALTASSAT, J.-M.,
1084 FABRIOL, H., BOURGEOIS, B., & LASNE, E. 2010. Assessment of the Bouillante
1085 Geothermal Field (Guadeloupe, French West Indies): Toward a Conceptual Model of the
1086 High Temperature Geothermal System. In: World Geothermal Congress 2010, April 2010.
1087 Bali, Indonesia, International Geothermal Association.
1088 BOUCHOT, V., GADALIA, A., TRAINEAU, H., & CARITG, S. 2014. Toward a Continuum
1089 Geothermal Model to Explain Coexistence of Medium to High (100 to 250 C) Temperature
1090 Geothermal Systems in Martinique and Guadeloupe. In: French West Indies–Proceedings
1091 Geothermal Research Council Annual Meeting. Portland, USA, 363–368.

1092 BOUDON, G., SEMET, M.P., & VINCENT, P.M. 1987. Magma and hydrothermally driven
1093 sector collapses: The 3100 and 11,500 y. B.P. eruptions of la Grande Decouverte (la
1094 Soufrière) volcano, Guadeloupe, French West Indies. Journal of Volcanology and
1095 Geothermal Research, 33, 317–323, doi: 10.1016/0377-0273(87)90021-7.
1096 BOUDON, G., KOMOROWSKI, J.C., VILLEMANT, B., & SEMET, M.P. 2008. A new scenario
1097 for the last magmatic eruption of La Soufrière of Guadeloupe (Lesser Antilles) in 1530 A.D.
1098 Evidence from stratigraphy radiocarbon dating and magmatic evolution of erupted products.
1099 Journal of Volcanology and Geothermal Research, 178, 474–490, doi:
1100 10.1016/j.jvolgeores.2008.03.006.
1101 BOUMA, A.H. 1962. Sedimentology of some Flysch Deposits: A Graphic Approach to Facies
1102 Interpretation. Elsevier, Amsterdam, 168.
1103 BOURDELLE, F. & CATHELINEAU, M. 2015. Low-temperature chlorite geothermometry: a
1104 graphical representation based on a T-R2+-Si diagram. European Journal of Mineralogy, 27,
1105 617–626, doi: 10.1127/ejm/2015/0027-2467.
1106 BOUYSSE, P. & GARRABÉ, F. 1984. Evolution tectonique néogène des îles calcaires de
1107 l'archipel de Guadeloupe. Comptes Rendus de l'Académie des Sciences de Paris, II, 763–
1108 766.
1109 BOUYSSE, P. & WESTERCAMP, D. 1988. Effets de la subduction de rides océaniques sur
1110 l'évolution d'un arc insulaire: l'exemple des Petites Antilles. Géologie de la France, 2/3, 2–38.
1111 BOUYSSE, P. & WESTERCAMP, D. 1990. Subduction of Atlantic aseismic ridges and Late
1112 Cenozoic evolution of the Lesser Antilles island arc. Tectonophysics, 175, 349–380, doi:
1113 10.1016/0040-1951(90)90180-G.
1114 BRODIE, K., FETTES, D., HARTE, B., & SCHMID, R. 2007. Structural Terms Including Fault
1115 Rock Terms - Recommendations by the IUGS Subcommission on the Systematics of
1116 Metamorphic Rocks.
1117 BROGI, A., LAZZAROTTO, A., LIOTTA, D., & RANALLI, G. 2003. Extensional shear zones
1118 as imaged by reflection seismic lines: the Larderello geothermal field (central Italy).
1119 Tectonophysics, 363, 127–139, doi: 10.1016/S0040-1951(02)00668-6.

1120 BROGI, A., LAZZAROTTO, A., LIOTTA, D., & RANALLI, G. 2005. Crustal structures in the
1121 geothermal areas of southern Tuscany (Italy): Insights from the CROP 18 deep seismic
1122 reflection lines. Journal of Volcanology and Geothermal Research, 148, 60–80, doi:
1123 10.1016/j.jvolgeores.2005.03.014.
1124 BROWNE, P.R.L. 1978. Hydrothermal alteration in active geothermal fields. Annual Review
1125 of Earth and Planetary Sciences, 6, 229–250.
1126 BROWNE, P.R.L. & ELLIS, A.J. 1970. The Ohaki-Broadlands hydrothermal area, New
1127 Zealand; mineralogy and related geochemistry. American Journal of Science, 269, 97–131,
1128 doi: 10.2475/ajs.269.2.97.
1129 BUCHER, K. & FREY, M. 2002. Petrogenesis of Metamorphic Rocks. Springer Science &
1130 Business Media.
1131 BULLER, A.T., BJØRKUM, P.A., NADEAU, P.H., & WALDERHAUG, O. 2005. Distribution of
1132 Hydrocarbons in Sedimentary Basins.
1133 CALCAGNO, P., BOUCHOT, V., THINON, I., & BOURGINE, B. 2012. A new 3D fault model
1134 of the Bouillante geothermal province combining onshore and offshore structural knowledge
1135 (French West Indies). Tectonophysics, 526–529, 185–195, doi: 10.1016/j.tecto.2011.08.012.
1136 CALCAGNO, P., BOUCHOT, V., THINON, I., BOURGINE, B., & GUILLEMIN, C. 2015. 3D
1137 Fault Model of the Bouillante Geothermal Province Interpreted from Onshore and Offshore
1138 Structural Knowledge (French West Indies). In: Proceedings World Geothermal Congress
1139 2015. 1–6.
1140 CAMELI, G.M., DINI, I., & LIOTTA, D. 1998. Brittle/ductile boundary from seismic reflection
1141 lines of southern Tuscany (Northern Apennines, Italy). Mem. Soc. Geol. Ital., 52, 153–163.
1142 CARIGNAN, J., HILD, P., MEVELLE, G., MOREL, J., & YEGHICHEYAN, D. 2001. Routine
1143 Analyses of Trace Elements in Geological Samples using Flow Injection and Low Pressure
1144 On-Line Liquid Chromatography Coupled to ICP-MS: A Study of Geochemical Reference
1145 Materials BR, DR-N, UB-N, AN-G and GH. Geostandards and Geoanalytical Research, 25,
1146 187–198, doi: 10.1111/j.1751-908X.2001.tb00595.x.

1147 CATHELINEAU, M. 1988. Cation site occupancy in chlorites and illites as a function of
1148 Temperature. Clay Minerals, 23, 471–485.
1149 CATHELINEAU, M. & NIEVA, D. 1985. A chlorite solid solution geothermometer the Los
1150 Azufres (Mexico) geothermal system. Contributions to Mineralogy and Petrology, 91, 235–
1151 244.
1152 CHAMBEFORT, I., LEWIS, B., SIMPSON, M.P., BIGNALL, G., RAE, A.J., & GANEFIANTO,
1153 N. 2017. Ngatamariki Geothermal System: Magmatic to Epithermal Transition in the Taupo
1154 Volcanic Zone, New Zealand. Economic Geology, 112, 319–346, doi:
1155 10.2113/econgeo.112.2.319.
1156 CHERKOSE, B.A. & MIZUNAGA, H. 2018. Resistivity imaging of Aluto-Langano geothermal
1157 field using 3-D magnetotelluric inversion. Journal of African Earth Sciences, 139, 307–318,
1158 doi: 10.1016/j.jafrearsci.2017.12.017.
1159 CLOOS, M. 1993. Lithospheric buoyancy and collisional orogenesis: Subduction of oceanic
1160 plateaus, continental margins, island arcs, spreading ridges, and seamounts. Geological
1161 Society of America Bulletin, 105, 715–737, doi: 10.1130/0016-
1162 7606(1993)105<0715:LBACOS>2.3.CO;2.
1163 COOKE, D.R. & SIMMONS, S.F. 2000. Characteristics and genesis of epithermal Au
1164 deposits. Reviews in Economic Geology, 13, 221–244.
1165 CORMY, G., DEMIANS D'ARCHIMBAUD, J., & SURCIN, J. 1970. Prospection geothermique
1166 aux antilles françaises, guadeloupe et Martinique. Geothermics, 2, 57–72, doi:
1167 10.1016/0375-6505(70)90006-4.
1168 CORSINI, M., LARDEAUX, J.M., VERATI, C., VOITUS, E., & BALAGNE, M. 2011. Discovery
1169 of lower cretaceous synmetamorphic thrust tectonics in French lesser antilles (La Désirade
1170 Island, Guadeloupe): Implications for Caribbean geodynamics. Tectonics, 30, 1–15, doi:
1171 10.1029/2011TC002875.
1172 COTTEN, J., LE DEZ, A., BAU, M., CAROFF, M., MAURY, R.C., DULSKI, P., FOURCADE,
1173 S., BOHN, M., & BROUSSE, R. 1995. Origin of anomalous rare-earth element and yttrium

1174 enrichments in subaerially exposed basalts: Evidence from French Polynesia. Chemical
1175 Geology, 119, 115–138, doi: 10.1016/0009-2541(94)00102-E.
1176 COYLE, B.J. & ZOBACK, M.D. 1988. In situ permeability and fluid pressure measurements
1177 at ~2 km depth in the Cajon Pass research well. Geophysical Research Letters, 15, 1029.
1178 DAGAIN, J., PATERNE, M., & WESTERCAMP, D. 1981. La mise en place du massif
1179 volcanique Madeleine-Soufrière, Basse-Terre de Guadeloupe, Antilles. Comptes Rendus de
1180 l'Academie des Sciences de Paris, 292, 921–926.
1181 DE CAPITANI, C. & PETRAKAKIS, K. 2010. The computation of equilibrium assemblage
1182 diagrams with Theriak/Domino software. American Mineralogist, 95, 1006–1016, doi:
1183 10.2138/am.2010.3354.
1184 DE MIN, L. 2014. Sismo-Stratigraphie Multi-Échelles d'un Bassin d'avant-Arc : Le Bassin de
1185 Marie-Galante, Petites Antilles. University of Antilles and Guyane, Pointe-à-Pitre,
1186 Guadeloupe.
1187 DE MIN, L., LEBRUN, J.-F., CORNÉE, J.-J., MÜNCH, P., LÉTICÉE, J.L., QUILLÉVÉRÉ, F.,
1188 MELINTE-DOBRINESCU, M., RANDRIANASOLO, A., MARCAILLOU, B., & ZAMI, F. 2015.
1189 Tectonic and sedimentary architecture of the Karukéra spur: A record of the Lesser Antilles
1190 fore-arc deformations since the Neogene. Marine Geology, 363, 15–37, doi:
1191 10.1016/j.margeo.2015.02.007.
1192 DEL MORO, A., PUXEDDU, M., RADICATI DI BROZOLO, F., & VILLA, I.M. 1982. Rb-Sr and
1193 K-Ar ages on minerals at temperatures of 300°-400°C from deep wells in the Larderello
1194 geothermal field (Italy). Contributions to Mineralogy and Petrology, 81, 340–349, doi:
1195 10.1007/BF00371688.
1196 DEMETS, C., JANSMA, P.E., MATTIOLI, G.S., DIXON, T.H., FARINA, F., BILHAM, R.,
1197 CALAIS, E., & MANN, P. 2000. GPS geodetic constraints on Caribbean-North America Plate
1198 Motion. Geophysical Research Letters, 27, 437–440, doi: 10.1029/1999GL005436.
1199 DEMIANS D'ARCHIMBAUD, J. & MUNIER-JOLAIN, J.P. 1976. Les Progrès de l'exploration
1200 Géothermique à Bouillante En Guadeloupe.

1201 DEMIANS D'ARCHIMBAUD, J. & SURCIN, J. 1976. Recherches géothermiques en
1202 Guadeloupe. Bulletin du Bureau de Recherches Géologiques et Minières.
1203 DESSERT, C., LAJEUNESSE, E., LLORET, E., CLERGUE, C., CRISPI, O., GORGE, C., &
1204 QUIDELLEUR, X. 2015. Controls on chemical weathering on a mountainous volcanic tropical
1205 island: Guadeloupe (French West Indies). Geochimica et Cosmochimica Acta, 171, 216–237,
1206 doi: 10.1016/j.gca.2015.09.009.
1207 DURNEY, D.W. 1972. Solution-transfer, an important geological deformation mechanism.
1208 Nature, 235, 315–317.
1209 DYSTHE, D.K. 2002. Fluid in mineral interfaces-molecular simulations of structure and
1210 diffusion. Geophysical Research Letters, 29, 1109, doi: 10.1029/2001GL013208.
1211 DYSTHE, D.K., RENARD, F., FEDER, J., JAMTVEIT, B., MEAKIN, P., & JØSSANG, T.
1212 2003. High-resolution measurements of pressure solution creep. Physical Review E, 68,
1213 011603, doi: 10.1103/PhysRevE.68.011603.
1214 EHRENBERG, S.N. 1993. Preservation of anomalous high porosity in deeply buried
1215 sandstones by grain-coating chlorite: examples from the Norwegian continental shelf.
1216 American Association of Petroleum Geologists Bulletin, 77, 1260–1286.
1217 ELLIOTT, D. 1973. Diffusion flow laws in metamorphic rocks. Geological Society of America
1218 Bulletin, 84, 2645–2664.
1219 ENGLAND, P. & WILKINS, C. 2004. A simple analytical approximation to the temperature
1220 structure in subduction zones. Geophysical Journal International, 159, 1138–1154, doi:
1221 10.1111/j.1365-246X.2004.02419.x.
1222 ERKAN, K. 2015. Geothermal investigations in western Anatolia using equilibrium
1223 temperatures from shallow boreholes. Solid Earth, 6, 103–113, doi: 10.5194/se-6-103-2015.
1224 ERNST, W.G. 1971. Do mineral parageneses reflect unusually high-pressure conditions of
1225 Franciscan metamorphism? American Journal of Science, 270, 81–108, doi:
1226 10.2475/ajs.270.2.81.

1227 FAMIN, V. & NAKASHIMA, S. 2005. Hydrothermal fluid venting along a seismogenic
1228 detachment fault in the Moresby rift (Woodlark basin, Papua New Guinea). Geochemistry,
1229 Geophysics, Geosystems, 6, 15, doi: 10.1029/2005GC001112.
1230 FAMIN, V., PHILIPPOT, P., JOLIVET, L., & AGARD, P. 2004. Evolution of hydrothermal
1231 regime along a crustal shear zone, Tinos Island, Greece. Tectonics, 23, 23, doi:
1232 10.1029/2003TC001509.
1233 FAVIER, A. 2019. Evolution Spatio-Temporelle de l'hydrothermalisme Dans La Plaque
1234 Supérieure de l'arc Des Petites Antilles En Guadeloupe. Applications Aux Systèmes
1235 Géothermaux. Université des Antilles, Pointe-à-Pitre, Guadeloupe.
1236 FAVIER, A., LARDEAUX, J.-M., LEGENDRE, L., VERATI, C., PHILIPPON, M., CORSINI,
1237 M., MÜNCH, P., & VENTALON, S. 2019. Tectono-metamorphic evolution of shallow crustal
1238 levels within active volcanic arcs. Insights from the exhumed Basal Complex of Basse-Terre
1239 (Guadeloupe, French West Indies). BSGF - Earth Sciences Bulletin, 190, 22, doi:
1240 10.1051/bsgf/2019011.
1241 FERMI, E. 1936. Thermodynamics. New-York, Dover Press.
1242 FEUILLET, N., MANIGHETTI, I., & TAPPONNIER, P. 2001. Extension active perpendiculaire
1243 à la subduction dans l'arc des Petites Antilles (Guadeloupe, Antilles françaises). Comptes
1244 Rendus de l'Academie de Sciences - Serie IIa: Sciences de la Terre et des Planetes, 333,
1245 583–590, doi: 10.1016/S1251-8050(01)01543-9.
1246 FEUILLET, N., MANIGHETTI, I., TAPPONNIER, P., & JACQUES, E. 2002. Arc parallel
1247 extension and localization of volcanic complexes in Guadeloupe, Lesser Antilles. Journal of
1248 Geophysical Research, 107 (B12), ETG 3 1-29, doi: 10.1029/2001JB000308.
1249 FEUILLET, N., TAPPONNIER, P., MANIGHETTI, I., VILLEMANT, B., & KING, G.C.P. 2004.
1250 Differential uplift and tilt of Pleistocene reef platforms and Quaternary slip rate on the Morne-
1251 Piton normal fault (Guadeloupe, French West Indies). Journal of Geophysical Research:
1252 Solid Earth, 109, 1–18, doi: 10.1029/2003JB002496.
1253 FEUILLET, N., LECLERC, F., TAPPONNIER, P., BEAUDUCEL, F., BOUDON, G., LE
1254 FRIANT, A., DEPLUS, C., LEBRUN, J.-F., NERCESSIAN, A., SAUREL, J.-M., & CLÉMENT,

1255 V. 2010. Active faulting induced by slip partitioning in Montserrat and link with volcanic
1256 activity: New insights from the 2009 GWADASEIS marine cruise data. Geophysical Research
1257 Letters, 37, n/a-n/a, doi: 10.1029/2010GL042556.
1258 FEUILLET, N., BEAUDUCEL, F., & TAPPONNIER, P. 2011. Tectonic context of moderate to
1259 large historical earthquakes in the Lesser Antilles and mechanical coupling with volcanoes.
1260 Journal of Geophysical Research: Solid Earth, 116, 1–26, doi: 10.1029/2011JB008443.
1261 FREY, M. & ROBINSON, D. 1999. Low-Grade Metamorphism. John Wiley & Sons (ed.).
1262 Oxford, Blackwell Science.
1263 FUKAHATA, Y. & MATSU'URA, M. 2000. Effects of active crustal movements on thermal
1264 structure in subduction zones. Geophysical Journal International, 141, 271–281, doi:
1265 10.1046/j.1365-246x.2000.00120.x.
1266 FULIGNATI, P., GIONCADA, A., & SBRANA, A. 1999. Rare-earth element (REE) behaviour
1267 in the alteration facies of the active magmatic–hydrothermal system of Vulcano (Aeolian
1268 Islands, Italy). Journal of Volcanology and Geothermal Research, 88, 325–342, doi:
1269 10.1016/S0377-0273(98)00117-6.
1270 FURUKAWA, Y. & UYEDA, S. 1989. Thermal state under the Tohoko arc with consideration
1271 of crustal heat generation. Tectonophysics, 164, 175–187, doi: 10.1016/0040-
1272 1951(89)90011-5.
1273 FURUKAWA, Y., SHINJOE, H., & NISHIMURA, S. 1998. Heat flow in the Southwest Japan
1274 Arc and its implication for thermal processes under arcs. Geophysical Research Letters, 25,
1275 1087–1090, doi: 10.1029/98GL00545.
1276 FYFE, W.S., PRICE, N.J., & THOMPSON, A.B. 1978. Fluids in the Earth's crust. In:
1277 Oxburgh, E. R. (ed.) Developments in Geochemistry, I. Amsterdam, Oxford, New-York,
1278 Cambridge University Press, 383.
1279 GAILLER, L.S., MARTELET, G., THINON, I., BOUCHOT, V., LEBRUN, J.F., & MÜNCH, P.
1280 2013. Crustal structure of Guadeloupe islands and the Lesser Antilles arc from a new gravity
1281 and magnetic synthesis. Bulletin de la Societe Geologique de France, 184, 77–97, doi:
1282 10.2113/gssgfbull.184.1-2.77.

1283 GARDEN, T.O., CHAMBEFORT, I., GRAVLEY, D.M., DEERING, C.D., & KENNEDY, B.M.
1284 2020. Reconstruction of the fossil hydrothermal system at Lake City caldera, Colorado,
1285 U.S.A.: Constraints for caldera-hosted geothermal systems. Journal of Volcanology and
1286 Geothermal Research, 393, 23, doi: 10.1016/j.jvolgeores.2020.106794.
1287 GARVEN, G. & RAFFENSPERGER, J.P. 1997. Hydrogeology and geochemistry of ore
1288 genesis in sedimentary basins. In: Barnes, H. L. (ed.) Geochemistry of Hydrothermal Ore
1289 Deposits - Third Edition. Wiley, 125–189.
1290 GRATIER, J.-P., GUIGUET, R., RENARD, F., JENATTON, L., & BERNARD, D. 2009. A
1291 pressure solution creep law for quartz from indentation experiments. Journal of Geophysical
1292 Research, 114, B03403, doi: 10.1029/2008JB005652.
1293 GRATIER, J.-P., DYSTHE, D.K., & RENARD, F. 2013. The Role of Pressure Solution Creep
1294 in the Ductility of the Earth's Upper Crust. In: Advances in Geophysics. 47–179., doi:
1295 10.1016/B978-0-12-380940-7.00002-0.
1296 GREEN, H.W. 1984. 'Pressure solution' creep: some causes and mechanisms. Journal of
1297 Geophysical Research-Solid Earth, 89, 4313–4318.
1298 GUILBERT, J.M. & PARK, C.F.J. 1986. The Geology of Ore Deposits. New York, W. H.
1299 Freeman and Compagny.
1300 GUILLOU-FROTTIER, L. 2003. Compilation et Analyse Des Données Thermiques Sur Le
1301 Champ Géothermique de Bouillante. Premières Interprétations Pour Le Fonctionnement Du
1302 Champ Géothermique. Rapport Final. BRGM/RP-52452-FR.
1303 HASEBE, K., FUJII, N., & UYEDA, S. 1970. Thermal processes under island arcs.
1304 Tectonophysics, 10, 335–355, doi: 10.1016/0040-1951(70)90114-9.
1305 HASTIE, A.R., KERR, A.C., PEARCE, J.A., & MITCHELL, S.F. 2007. Classification of altered
1306 volcanic island arc rocks using immobile trace elements: Development of the Th-Co
1307 discrimination diagram. Journal of Petrology, 48, 2341–2357, doi:
1308 10.1093/petrology/egm062.
1309 HAWKESWORTH, C.J. & POWELL, M. 1980. Magma genesis in the lesser Antilles island
1310 arc. Earth and Planetary Science Letters, 51, 297–308, doi: 10.1016/0012-821X(80)90212-5.

1311 HEDENQUIST, J.W. 1986. Mineralization associated with volcanic-related hydrothermal
1312 systems in the Circum-Pacific basin. Transactions of the Fourth Circum Pacific Energy and
1313 Mineral Ressources Conference, American Association of Petroleum Geologists, Chapter 44,
1314 513–524.
1315 HENLEY, R.W. & ELLIS, A.J. 1983. Geothermal systems ancient and modern: a
1316 geochemical review. Earth-Science Reviews, 19, 1–50, doi: 10.1016/0012-8252(83)90075-2.
1317 HENLEY, R.W., HEDENQUIST, J.W., & ROBERTS, P.J. 1986. Guide to the Active
1318 Epithermal (Geothermal) Systems and Precious Metal Deposits of New Zealand,
1319 Monograph.
1320 HOBBS, B.E., MEANS, W.D., & WILLIAMS, P.F. 1976. An Outline of Structural Geology,
1321 Wiley and.
1322 HOLLAND, T.J.B. & POWELL, R. 2004. An internally consistent thermodynamic data set for
1323 phases of petrological interest. Journal of Metamorphic Geology, 16, 309–343, doi:
1324 10.1111/j.1525-1314.1998.00140.x.
1325 IUNDT, F. & OUZOUNIAN, G. 1984. Prospection Géothermique de La Région de Bouillante -
1326 Vieux Habitants Guadeloupe, Rapport Du B.R.G.M 84 SGN 063 GTH. Orléans, France.
1327 JACQUES, D. & MAURY, R.C. 1988. Carte géologique au 1/20 000e, département de la
1328 Guadeloupe, Les Saintes. BRGM, Service Géologique National, Orléans.
1329 JACQUES, D., MAURY, R.C., & BELLON, H. 1984. Geology and K-Ar geochronology of Les
1330 Saintes island, guadeloupe, Frend West-Indies Géologie et géochronologie 40K-40Ar des
1331 îles des Saintes (Guadeloupe). Gauthier-Villars.
1332 JAEGER, J.C. 1969. Elasticity, Fracture and Flow, 3rd Ed. London, Butler & Tanner Ltd.
1333 JAEGER, J.C. & COOK, N.G.W. 1979. Fundamental of Rock Mechanics, Third Ed. Chapman
1334 and Hall.
1335 JAEGER, J.C., COOK, N.G., & ZIMMERMAN, R. 2009. Fundamentals of Rock Mechanics,
1336 4th Edition. Blackwell Publishing Ltd.
1337 JI, J. & BROWNE, P.R.L. 2000. Relationship between illite crystallinity and temperature in
1338 active geothermal systems of New Zealand. Clays and Clay Minerals, 48, 139–144.

1339 JOSEPH, PHILIPPE & LOMAS, SIMON A. 2004. Deep-water sedimentation in the Alpine
1340 Foreland Basin of SE France: New perspectives on the Grès d'Annot and related systems—
1341 an introduction Joseph, P & Lomas, S A (eds). Geological Society, London, Special
1342 Publications, 221, 1–16, doi: 10.1144/GSL.SP.2004.221.01.01.
1343 JULIEN, P. & BONNETON, J.-R. 1989. Regional stress field in the Lesser Antilles between
1344 Guadeloupe and Barbuda Islands. Geophysical Research Letters, 16, 1313–1316, doi:
1345 10.1029/GL016i011p01313.
1346 KAYA, A. 2015. The effects of extensional structures on the heat transport mechanism: An
1347 example from the Ortakçı geothermal field (Büyük Menderes Graben, SW Turkey). Journal of
1348 African Earth Sciences, 108, 74–88, doi: 10.1016/j.jafrearsci.2015.05.002.
1349 KERRICH, R., FYFE, W.S., GORMAN, B.E., & ALLISON, I. 1977. Local modification of rock
1350 chemistry by deformation. Contributions to Mineralogy and Petrology, 65, 183–190.
1351 KIRBY, S.H. 1983. Rheology of the lithosphere. Reviews of Geophysics, 21, 1458, doi:
1352 10.1029/RG021i006p01458.
1353 KLEIN, D.P. & JOHNSON, G.R. 1983. Density, Porosity and Magnetic Properties of Rock
1354 Specimens from Southwestern Arizona.
1355 KONDEPUDI, D. & PRIGOGINE, I. 1998. MODERN THERMODYNAMICS -From Heat
1356 Engines to Dissipative Structures. John Wiley & Sons.
1357 KOPP, H., WEINZIERL, W., BECEL, A., CHARVIS, P., EVAIN, M., FLUEH, E.R., GAILLER,
1358 A., GALVE, A., HIRN, A., KANDILAROV, A., KLAESCHEN, D., LAIGLE, M., PAPENBERG,
1359 C., PLANERT, L., & ROUX, E. 2011. Deep structure of the central Lesser Antilles Island Arc:
1360 Relevance for the formation of continental crust. Earth and Planetary Science Letters, 304,
1361 121–134, doi: 10.1016/j.epsl.2011.01.024.
1362 KORZHINSKII, D.S. 1965. The theory of systems with perfectly mobile components and
1363 processes of mineral formation. American Journal of Science, 263, 193–205, doi:
1364 10.2475/ajs.263.3.193.
1365 KRETZ, R. 1983. Symbols for rock-forming minerals. American Mineralogist, 68, 277–279.

1366 LABANIEH, S. 2009. Géochimie de l'île de La Martinique Aux Petites Antilles. Université
1367 Joseph-Fourier - Grenoble I, Grenoble.
1368 LACHASSAGNE, P., MARÉCHAL, J., & SANJUAN, B. 2009. Hydrogeological model of a
1369 high energy geothermal field (Bouillante area, Guadeloupe, French West Indies).
1370 Hydrogeology Journal, Springer Verlag, 17, 1589–1606.
1371 LAGAT, J. 2014. Hydrothermal Alteration Mineralogy in Geothermal Fields With Case
1372 Examples From Olkaria Domes Geothermal Field , Kenya. In: Short Course IX on
1373 Exploration for Geothermal Resources. Lake Bogoria and Lake Naivasha, Kenya, 1–24.
1374 LAIGLE, M., BECEL, A., DE VOOGD, B., SACHPAZI, M., BAYRAKCI, G., LEBRUN, J.-F., &
1375 EVAIN, M. 2013. Along-arc segmentation and interaction of subducting ridges with the
1376 Lesser Antilles Subduction forearc crust revealed by MCS imaging. Tectonophysics, 603,
1377 32–54, doi: 10.1016/j.tecto.2013.05.028.
1378 LANARI, P., WAGNER, T., & VIDAL, O. 2014. A thermodynamic model for di-trioctahedral
1379 chlorite from experimental and natural data in the system MgO-FeO-Al2O3-SiO2-H2O:
1380 Applications to P-T sections and geothermometry. Contributions to Mineralogy and
1381 Petrology, 167, 1–19, doi: 10.1007/s00410-014-0968-8.
1382 LARDEAUX, J.M., MÜNCH, P., CORSINI, M., CORNÉE, J.-J., VERATI, C., LEBRUN, J.-F.,
1383 QUILLÉVÉRÉ, F., MELINTE-DOBRINESCU, M., LÉTICÉE, J.L., FIETZKE, J.,
1384 MAZABRAUD, Y., CORDEY, F., & RANDRIANASOLO, A. 2013. La Désirade island
1385 (Guadeloupe, French West Indies): A key target for deciphering the role of reactivated
1386 tectonic structures in Lesser Antilles arc building. Bulletin de la Societe Geologique de
1387 France, 184, 21–34, doi: 10.2113/gssgfbull.184.1-2.21.
1388 LECLERC, F. & FEUILLET, N. 2019. Quaternary coral reef complexes as powerful markers
1389 of long-term subsidence related to deep processes at subduction zones: Insights from Les
1390 Saintes (Guadeloupe, French West Indies). Geosphere, 15, 983–1007, doi:
1391 10.1130/GES02069.1.
1392 LECLERC, F., FEUILLET, N., & DEPLUS, C. 2016. Interactions between active faulting,
1393 volcanism, and sedimentary processes at an island arc: Insights from Les Saintes channel,

1394 Lesser Antilles arc. Geochemistry, Geophysics, Geosystems, 17, 2781–2802, doi:
1395 10.1002/2016GC006337.
1396 LEDRU, P. & GUILLOU-FROTTIER, L. 2010. Reservoir Definition. In: Huenges, E. (ed.)
1397 Geothermal Energy Systems: Exploration, Development, and Utilization. Potsdam, Germany,
1398 1–36.
1399 LEGENDRE, L. 2018. Evolution Tectonique Du Nord de l'arc Des Petites Antilles. Université
1400 des Antilles, Pointe-à-Pitre, Guadeloupe.
1401 LEGENDRE, L., PHILIPPON, M., MÜNCH, P., LETICÉE, J.L., NOURY, M., MAINCENT, G.,
1402 CORNÉE, J.J., CARAVATI, A., LEBRUN, J.F., & MAZABRAUD, Y. 2018. Trench Bending
1403 Initiation: Upper Plate Strain Pattern and Volcanism. Insights From the Lesser Antilles Arc,
1404 St. Barthelemy Island, French West Indies. Tectonics, 37, 2777–2797, doi:
1405 10.1029/2017TC004921.
1406 LIOTTA, D. & BROGI, A. 2020. Pliocene-Quaternary fault kinematics in the Larderello
1407 geothermal area (Italy): Insights for the interpretation of the present stress field.
1408 Geothermics, 83, 21, doi: 10.1016/j.geothermics.2019.101714.
1409 LIOTTA, D. & RANALLI, G. 1999. Correlation between seismic reflectivity and rheology in
1410 extended lithosphere: southern Tuscany, inner Northern Apennines, Italy. Tectonophysics,
1411 315, 109–122, doi: 10.1016/S0040-1951(99)00292-9.
1412 LIOTTA, D., RUGGIERI, G., BROGI, A., FULIGNATI, P., DINI, A., & NARDINI, I. 2010.
1413 Migration of geothermal fluids in extensional terrains: the ore deposits of the Boccheggiano-
1414 Montieri area (southern Tuscany, Italy). International Journal of Earth Sciences, 99, 623–
1415 644, doi: 10.1007/s00531-008-0411-3.
1416 LIOU, J.G., MAUYAMA, S., & CHO, M. 1987. Very low-grade metamorphism of volcanic and
1417 volcaniclastic rocks-mineral assemblages and mineral facies. In: Frey, M. (ed.) Low
1418 Temperature Metamorphism. Blackie, Glasgow, 59–113.
1419 LLORET, E., DESSERT, C., GAILLARDET, J., ALBÉRIC, P., CRISPI, O., CHADUTEAU, C.,
1420 & BENEDETTI, M.F. 2011. Comparison of dissolved inorganic and organic carbon yields and

1421 fluxes in the watersheds of tropical volcanic islands, examples from Guadeloupe (French
1422 West Indies). Chemical Geology, 280, 65–78, doi: 10.1016/j.chemgeo.2010.10.016.
1423 LÓPEZ, A.M., STEIN, S., DIXON, T., SELLA, G., CALAIS, E., JANSMA, P., WEBER, J., &
1424 LAFEMINA, P. 2006. Is there a northern Lesser Antilles forearc block? Geophysical
1425 Research Letters, 33, 2–5, doi: 10.1029/2005GL025293.
1426 MANGA, M., HORNBACH, M.J., LE FRIANT, A., ISHIZUKA, O., STRONCIK, N., ADACHI,
1427 T., ALJAHDALI, M., BOUDON, G., BREITKREUZ, C., FRAASS, A., FUJINAWA, A.,
1428 HATFIELD, R., JUTZELER, M., KATAOKA, K., LAFUERZA, S., MAENO, F., MARTINEZ-
1429 COLON, M., MCCANTA, M., MORGAN, S., PALMER, M.R., SAITO, T., SLAGLE, A.,
1430 STINTON, A.J., SUBRAMANYAM, K.S. V, TAMURA, Y., TALLING, P.J., VILLEMANT, B.,
1431 WALL-PALMER, D., & WANG, F. 2012. Heat flow in the Lesser Antilles island arc and
1432 adjacent back arc Grenada basin. Geochemistry, Geophysics, Geosystems, 13, 1–19, doi:
1433 10.1029/2012GC004260.
1434 MAS, A., GUISSEAU, D., PATRIER MAS, P., BEAUFORT, D., GENTER, A., SANJUAN, B.,
1435 & GIRARD, J.P. 2006. Clay minerals related to the hydrothermal activity of the Bouillante
1436 geothermal field (Guadeloupe). Journal of Volcanology and Geothermal Research, 158, 380–
1437 400, doi: 10.1016/j.jvolgeores.2006.07.010.
1438 MASON, R. 1978. Petrology of the Metamorphic Rocks. Kluwer Academic Publishers.
1439 MATHIEU, L., VAN WYK DE VRIES, B., PILATO, M., & TROLL, V.R. 2011. The interaction
1440 between volcanoes and strike-slip, transtensional and transpressional fault zones: Analogue
1441 models and natural examples. Journal of Structural Geology, 33, 898–906, doi:
1442 10.1016/j.jsg.2011.03.003.
1443 MAURY, R.C., WESTBROOK, G.K., BAKER, P.E., BOUYSSE, P., & WESTERCAMP, D.
1444 1990. Chapter 5: Geology of the Lesser Antilles. In: Dengo, G. & Case, J. E. (eds) The
1445 Geology of North America, Vol. H. Boulder, Colorado, 141–166.
1446 MCCAIG, A.M. 1988. Deep fluid circulation in fault zones. Geology, 16, 867, doi:
1447 10.1130/0091-7613(1988)016<0867:DFCIFZ>2.3.CO;2.

1448 MCKENZIE, D.P. & SCLATER, J.G. 1968. Heat flow inside the Island Arcs of the
1449 northwestern Pacific. Journal of Geophysical Research, 73, 3173–3179, doi:
1450 10.1029/JB073i010p03173.
1451 MEYER, C. & HEMLEY, J.J. 1967. Wall rock alteration. In: Geochemistry of Hydrothermal
1452 Ore Deposits. New-York, 166–235.
1453 MICHARD, A., ALBARÈDE, F., MICHARD, G., MINSTER, J.F., & CHARLOU, J.L. 1983.
1454 Rare-earth elements and uranium in high-temperature solutions from East Pacific Rise
1455 hydrothermal vent field (13 °N). Nature, 303, 795–797, doi: 10.1038/303795a0.
1456 MIDDLETON, G. V. & BOUMA, A.H. 1973. Turbidites and Deep Water Sedimentation:
1457 Frontmatter. In: Geology, S. for S. (ed.) SEPM Pacific Section Short Course. Anaheim.
1458 MILLOT, R., SCAILLET, B., & SANJUAN, B. 2010. Lithium isotopes in island arc geothermal
1459 systems: Guadeloupe, Martinique (French West Indies) and experimental approach.
1460 Geochimica et Cosmochimica Acta, 74, 1852–1871, doi: 10.1016/j.gca.2009.12.007.
1461 MIYASHIRO, A. 1961. Evolution of Metamorphic Belts. Journal of Petrology, 2, 277–311, doi:
1462 10.1093/petrology/2.3.277.
1463 MOECK, I.S. 2014. Catalog of geothermal play types based on geologic controls. Renewable
1464 and Sustainable Energy Reviews, 37, 867–882, doi: 10.1016/j.rser.2014.05.032.
1465 MOULAS, E., SCHMALHOLZ, S.M., PODLADCHIKOV, Y., TAJČMANOVÁ, L.,
1466 KOSTOPOULOS, D., & BAUMGARTNER, L. 2019. Relation between mean stress,
1467 thermodynamic, and lithostatic pressure. Journal of Metamorphic Geology, 37, 1–14, doi:
1468 10.1111/jmg.12446.
1469 MULCH, A., TEYSSIER, C., COSCA, M.A., & VENNEMANN, T.W. 2006. Thermomechanical
1470 analysis of strain localization in a ductile detachment zone. Journal of Geophysical
1471 Research: Solid Earth, 111, 20, doi: 10.1029/2005JB004032.
1472 MUNCH, P., LEBRUN, J.F., CORNÉE, J.-J., THINON, I., GUENNOC, P., MARCAILLOU,
1473 B.J., BEGOT, J., BERTRAND, G., DE BERC, S.B., BISCARRAT, K., CLAUD, C., DE MIN,
1474 L., FOURNIER, F., GAILLER, L., GRAINDORGE, D., LÉTICÉE, J.L., MARIE, L.,
1475 MAZABRAUD, Y., MELINTE-DOBRINESCU, M., MOISSETTE, P., QUILLÉVÉRÉ, F.,

1476 VERATI, C., & RANDRIANASOLO, A. 2013. Pliocene to Pleistocene carbonate systems of
1477 the Guadeloupe archipelago, french lesser antilles: A land and sea study (the KaShallow
1478 project). Bulletin de la Societe Geologique de France, 184, 99–110, doi:
1479 10.2113/gssgfbull.184.1-2.99.
1480 NADEAU, P.H. 2011. Earth's Energy 'Golden Zone': A Synthesis from Mineralogical
1481 Research. Clay Minerals, 46, 1–24.
1482 NADEAU, P.H. & EHRENBERG, S.N. 2006. Sandstone vs. carbonate petroleum reservoirs:
1483 A global perspective on porosity-depth and porosity-permeability relationships: Reply. AAPG
1484 Bulletin, 90, 811–813, doi: 10.1306/11070505163.
1485 NAVELOT, V. 2018. Caractérisations Structurale et Pétrophysique d'un Système
1486 Géothermique En Contexte Volcanique d'arc de Subduction. Exemple de l'archipel de
1487 Guadeloupe. Université de Lorraine.
1488 NAVELOT, V., GÉRAUD, Y., FAVIER, A., DIRAISON, M., CORSINI, M., LARDEAUX, J.-M.,
1489 VERATI, C., MERCIER DE LÉPINAY, J., LEGENDRE, L., & BEAUCHAMPS, G. 2018.
1490 Petrophysical properties of volcanic rocks and impacts of hydrothermal alteration in the
1491 Guadeloupe Archipelago (West Indies). Journal of Volcanology and Geothermal Research,
1492 360, 1–21, doi: 10.1016/j.jvolgeores.2018.07.004.
1493 NEUENDORF, K. K. E., J.P., JR., M., & JACKSON, J.A. 2005. Glossary of Geology, 5th
1494 Edition. Alexandria, Virginia, American Geological Institute.
1495 NICOLAS, A. & POIRIER, J.P. 1976. Crystalline Plasticity and Solid-State Flow in
1496 Metamorphic Rocks, Interscien. Wiley, J. (ed.). London.
1497 NOR, A. & WALDER, J. 1992. Chapter 19 Hydraulic Pulses in the Earth's Crust. In: Evans,
1498 B. & Wong, T. (eds) Fault Mechanics and Transport Properties of Rocks. International
1499 Geophysics, 461–473., doi: 10.1016/S0074-6142(08)62834-X.
1500 OLIVER, N.H.S. 1996. Review and classification of structural controls on fluid flow during
1501 regional metamorphism. Journal of Metamorphic Geology, 14, 477–492, doi: 10.1046/j.1525-
1502 1314.1996.00347.x.

1503 OXBURGH, E.R. & TURCOTTE, D.L. 1970. Thermal structure of island arcs. GSA bulletin,
1504 81, 1665–1688, doi: https://doi.org/10.1130/0016-7606(1970)81[1665:TSOIA]2.0.CO;2.
1505 PANDARINATH, K., DULSKI, P., TORRES-ALVARADO, I.S., & VERMA, S.P. 2008. Element
1506 mobility during the hydrothermal alteration of rhyolitic rocks of the Los Azufres geothermal
1507 field, Mexico. Geothermics, 37, 53–72, doi: 10.1016/j.geothermics.2007.10.002.
1508 PASSCHIER, C.W. & TROUW, R.A.J. 2005. Microtectonics, 2nd Ed. Springer, Berlin,
1509 Heidelberg.
1510 PECCERILLO, A. & TAYLOR, S.R. 1976. Geochemistry of eocene calc-alkaline volcanic
1511 rocks from the Kastamonu area, Northern Turkey. Contributions to Mineralogy and Petrology,
1512 58, 63–81, doi: 10.1007/BF00384745.
1513 PIRAJNO, F. 2009. Hydrothermal Processes and Mineral Systems - Volume I. Dordrecht,
1514 Springer Netherlands, doi: 10.1007/978-1-4020-8613-7.
1515 POIRIER, J.P. 1985. High-Temperature Deformation Processes in Metals, Ceramics and
1516 Minerals. Cambridge University Press.
1517 POWELL, C.M. 1979. A morphological classification of rock cleavage. Tectonophysics, 58,
1518 21–34, doi: 10.1016/0040-1951(79)90320-2.
1519 POWELL, R., HOLLAND, T., & WORLEY, B. 1998. Calculating phase diagrams involving
1520 solid solutions via non - linear equations, with examples using THERMOCALC. Journal of
1521 Metamorphic Geology, 16, 577–588, doi: 10.1111/j.1525-1314.1998.00157.x.
1522 PRÉCIGOUT, J., PRIGENT, C., PALASSE, L., & POCHON, A. 2017. Water pumping in
1523 mantle shear zones. Nature Communications, 8, 10, doi: 10.1038/ncomms15736.
1524 RAD, S., RIVÉ, K., VITTECOQ, B., CERDAN, O., & ALLÈGRE, C.J. 2013. Chemical
1525 weathering and erosion rates in the Lesser Antilles: An overview in Guadeloupe, Martinique
1526 and Dominica. Journal of South American Earth Sciences, 45, 331–344, doi:
1527 10.1016/j.jsames.2013.03.004.
1528 RAMBERG, H. 1952. Chemical Bonds and Distribution of Cations in Silicates. The Journal of
1529 Geology, 60, 331–355.

1530 RAMSAY, J.G. 1967. Folding and Fracturing of Rocks, MacGraw-Hi.
1531 RANALLI, G. & RYBACH, L. 2005. Heat flow, heat transfer and lithosphere rheology in
1532 geothermal areas: Features and examples. Journal of Volcanology and Geothermal
1533 Research, 148, 3–19, doi: 10.1016/j.jvolgeores.2005.04.010.
1534 RENARD, F., BROSSE, ., & GRATIER, J.P. 2000. The Different Processes Involved in the
1535 Mechanism of Pressure Solution in Quartz-Rich Rocks and their Interactions. In: Worden, R.
1536 H. & Morad, S. (eds) Quartz Cementation in Sandstones. Oxford, UK, Blackwell Publishing
1537 Ltd., 67–78., doi: 10.1002/9781444304237.ch5.
1538 REYES, A.G. 1990. Petrology of Philippine geothermal systems and the application of
1539 alteration mineralogy to their assessment. Journal of Volcanology and Geothermal Research,
1540 43, 279–309, doi: 10.1016/0377-0273(90)90057-M.
1541 RIBE, N.M. 1989. Seismic anisotropy and mantle flow. Journal of Geophysical Research:
1542 Solid Earth, 94, 4213–4223, doi: 10.1029/JB094iB04p04213.
1543 RICCI, J., LAHITTE, P., & QUIDELLEUR, X. 2015a. Construction and destruction rates of
1544 volcanoes within tropical environment: Examples from the Basse-Terre Island (Guadeloupe,
1545 Lesser Antilles). Geomorphology, 228, 597–607, doi: 10.1016/j.geomorph.2014.10.002.
1546 RICCI, J., QUIDELLEUR, X., & LAHITTE, P. 2015b. Volcanic evolution of central Basse-
1547 Terre Island revisited on the basis of new geochronology and geomorphology data. Bulletin
1548 of Volcanology, 77, 84, doi: 10.1007/s00445-015-0970-7.
1549 RICCI, J., QUIDELLEUR, X., PALLARES, C., & LAHITTE, P. 2017. High-resolution K-Ar
1550 dating of a complex magmatic system: The example of Basse-Terre Island (French West
1551 Indies). Journal of Volcanology and Geothermal Research, 345, 142–160, doi:
1552 10.1016/j.jvolgeores.2017.07.013.
1553 ROCHE, V., STERNAI, P., GUILLOU-FROTTIER, L., MENANT, A., JOLIVET, L.,
1554 BOUCHOT, V., & GERYA, T. 2018. Emplacement of metamorphic core complexes and
1555 associated geothermal systems controlled by slab dynamics. Earth and Planetary Science
1556 Letters, 498, 322–333, doi: 10.1016/j.epsl.2018.06.043.

1557 ROWLAND, J. V. & SIMMONS, S.F. 2012. Hydrologic, Magmatic, and Tectonic Controls on
1558 Hydrothermal Flow, Taupo Volcanic Zone, New Zealand: Implications for the Formation of
1559 Epithermal Vein Deposits. Economic Geology, 107, 427–457, doi:
1560 10.2113/econgeo.107.3.427.
1561 RUTTER, E.H. 1972. The effects of strain-rate changes on the strength and ductility of
1562 Solenhofen limestone at low temperatures and confining pressures. International Journal
1563 Rock Mechanics and Mining Sciences, 9, 183–189.
1564 RUTTER, E.H. 1976. The kinetics of rock deformation by pressure solution. Philosophical
1565 Transactions of the Royal Society London, 283, 203–219, doi: 10.1098/rsta.1976.0079.
1566 RUTTER, E.H. 1983. Pressure solution in nature, theory and experiment. Journal of the
1567 Geological Society, 140, 725–740, doi: 10.1144/gsjgs.140.5.0725.
1568 SACHAU, T., BONS, P.D., & GOMEZ-RIVAS, E. 2015. Transport efficiency and dynamics of
1569 hydraulic fracture networks. Frontiers in Physics, 3, 13, doi: 10.3389/fphy.2015.00063.
1570 SAK, P.B., NAVARRE-SITCHLER, A.K., MILLER, C.E., DANIEL, C.C., GAILLARDET, J.,
1571 BUSS, H.L., LEBEDEVA, M.I., & BRANTLEY, S.L. 2010. Controls on rind thickness on
1572 basaltic andesite clasts weathering in Guadeloupe. Chemical Geology, 276, 129–143, doi:
1573 10.1016/j.chemgeo.2010.05.002.
1574 SALAÜN, A., VILLEMANT, B., GÉRARD, M., KOMOROWSKI, J.-C., & MICHEL, A. 2011.
1575 Hydrothermal alteration in andesitic volcanoes: Trace element redistribution in active and
1576 ancient hydrothermal systems of Guadeloupe (Lesser Antilles). Journal of Geochemical
1577 Exploration, 111, 59–83, doi: 10.1016/j.gexplo.2011.06.004.
1578 SAMPER, A., QUIDELLEUR, X., LAHITTE, P., & MOLLEX, D. 2007. Timing of effusive
1579 volcanism and collapse events within an oceanic arc island: Basse-Terre, Guadeloupe
1580 archipelago (Lesser Antilles Arc). Earth and Planetary Science Letters, 258, 175–191, doi:
1581 10.1016/j.epsl.2007.03.030.
1582 SANJUAN, B. & BRACH, M. 1997. Etude Hydrogéochimique Du Champ Géothermique de
1583 Bouillante (Guadeloupe). Orléans, France.

1584 SANJUAN, B., BRACH, M., & LASNE, E. 2001. Bouillante geothermal fluid: mixing and
1585 water/rock interaction processes at 250°C. In: Cidu, R. (ed.) Proceedings of the 10th
1586 International Symposium on Water/Rock Interactions (WRI10), Vol. 2, 10-15 July 2001.
1587 Villasimius, Italy, A.A. Balkema publishers, 911–914.
1588 SANJUAN, B., LE NINDRE, Y.M., MENJOZ, A., SBAI, A., BRACH, M., & LASNE, E. 2004.
1589 Travaux de Recherche Liés Au Développement Du Champ Géothermique de Bouillante
1590 (Guadeloupe), Report BRGM/RP-53136-FR. Orléans, France.
1591 SANJUAN, B., MILLOT, R., BRACH, M., ASMUNDSSON, R., & GIROUD, N. 2010. Use of a
1592 New Sodium/Lithium (Na/Li) Geothermometric Relationship for High-Temperature Dilute
1593 Geothermal Fluids from Iceland. In: World Geothermal Congress 2010, Apr 2010, Bali,
1594 Indonesia. 12.
1595 SCHIFFMAN, P., ELDERS, W.A., WILLIAMS, A.E., MCDOWELL, S.D., & BIRD, D.K. 1984.
1596 Active metasomatism in the Cerro Prieto geothermal system, Baja California, Mexico: A
1597 telescoped low-pressure, low-temperature metamorphic facies series. Geology, 12, 12, doi:
1598 10.1130/0091-7613(1984)12<12:AMITCP>2.0.CO;2.
1599 SCHIFFMAN, P., BETTISON, L., & WILLIAMS, A. 1986. Hydrothermal metamorphism of the
1600 Point Sal remnant, California Coast Range ophiolite. In: Proceedings of the Fifth International
1601 Symposium on Water-Rock Interactions. 489–492.
1602 SCHIFFMAN, P., EVARTS, R.C., WILLIAMS, A.E., & PICKTHORN, W.J. 1991.
1603 Hydrothermal Metamorphism in Oceanic Crust from the Coast Range Ophiolite of California:
1604 Fluid-Rock Interaction in a Rifted Island Arc. 399–425., doi: 10.1007/978-94-011-3358-6_20.
1605 SCLATER, J.G. 1972. Heat flow and elevation of the marginal basins of the western Pacific.
1606 Journal of Geophysical Research, 77, 5705–5719, doi: 10.1029/JB077i029p05705.
1607 SIBSON, R.H. & ROWLAND, J. V. 2003. Stress, fluid pressure and structural permeability in
1608 seismogenic crust, North Island, New Zealand. Geophysical Journal International, 154, 584–
1609 594, doi: 10.1046/j.1365-246X.2003.01965.x.

1610 SIBSON, R.H., MOORE, J.M.M., & RANKIN, A.H. 1975. Seismic pumping—a hydrothermal
1611 fluid transport mechanism. Journal of the Geological Society, 131, 653–659, doi:
1612 10.1144/gsjgs.131.6.0653.
1613 SIDDANS, A.W.B. 1972. Slaty cleavage - A review of research since 1815. Earth Science
1614 Review, 8, 205–232.
1615 SMULIKOWSKI W., DESMONS, J., FETTES, D.J., HARTE, B., SASSI, F.P., & SCHMID, R.
1616 2007. A systematic nomenclature for metamorphic rocks. 2. Types, grades and facies of
1617 metamorphism. Recommendations by the IUGS Subcommission on the Systematics of
1618 Metamorphic Rocks: Web version 01.02.07. SCMR website. World Wide Web Address:
1619 www.bgs.ac.uk/scmr/home.html.
1620 SORBY, H.C. 1863. On the direct correlation of mechanical and chemical forces. In:
1621 Proceeding of the Royal Society of London. 538–550.
1622 SPEAR, F.S. 1993. Metamorphic Phase Equilibria And Presure-Temperature-Time-Paths,
1623 Monograph. Washington, Mineralogical Society of America.
1624 STURCHIO, N.C., MUEHLENBACHS, K., & SEITZ, M.G. 1986. Element redistribution during
1625 hydrothermal alteration of rhyolite in an active geothermal system: Yellowstone drill cores Y-
1626 7 and Y-8. Geochimica et Cosmochimica Acta, 50, 1619–1631, doi: 10.1016/0016-
1627 7037(86)90125-0.
1628 SUN, S. -S. & MCDONOUGH, W.F. 1989. Chemical and isotopic systematics of oceanic
1629 basalts: implications for mantle composition and processes. Geological Society, London,
1630 Special Publications, 42, 313–345, doi: 10.1144/GSL.SP.1989.042.01.19.
1631 TAYLOR, S.R. & MCLENNAN, S.M. 1995. The geochemical evolution of the continental
1632 crust. Reviews of Geophysics, 33, 241, doi: 10.1029/95RG00262.
1633 TAYLOR, T.R., GILES, M.R., HATHON, L.A., DIGGS, T.N., BRAUNSDORF, N.R.,
1634 BIRBIGLIA, G. V., KITTRIDGE, M.G., MACAULAY, C.I., & ESPEJO, I.S. 2010. Sandstone
1635 diagenesis and reservoir quality prediction: Models, myths, and reality. AAPG Bulletin, 94,
1636 1093–1132, doi: 10.1306/04211009123.

1637 THINON, I., GUENNOC, P., BITRI, A., & TRUFFERT, C. 2010. Study of the Bouillante Bay
1638 (West Basse-Terre Island shelf): contribution of geophysical surveys to the understanding of
1639 the structural context of Guadeloupe (French West Indies - Lesser Antilles). Bulletin de la
1640 Societe Geologique de France, 181, 51–65, doi: 10.2113/gssgfbull.181.1.51.
1641 VAN RUTH, P. & HILLIS, R. 2000. Estimating pore pressure in the Cooper Basin, South
1642 Australia: sonic log method in an uplifted basin. Exploration Geophysics, 31, 441–447.
1643 VERATI, C., MAZABRAUD, Y., LARDEAUX, J.-M., CORSINI, M., SCHNEIDER, D., VOITUS,
1644 E., & ZAMI, F. 2016. Tectonic evolution of Les Saintes archipelago (Guadeloupe, French
1645 West Indies): relation with the Lesser Antilles arc system. Bulletin de la Société Géologique
1646 de France, 187, 3–10, doi: 10.2113/gssgfbull.187.1.3.
1647 VERATI, C., LARDEAUX, J.-M., FAVIER, A., CORSINI, M., PHILIPPON, M., & LEGENDRE,
1648 L. 2018. Arc-related metamorphism in the Guadeloupe archipelago (Lesser Antilles active
1649 island arc): First report and consequences. Lithos, 320–321, 592–598, doi:
1650 10.1016/j.lithos.2018.08.005.
1651 WATANABE, T., EPP, D., UYEDA, S., LANGSETH, M., & YASUI, M. 1970. Heat flow in the
1652 Philippine Sea. Tectonophysics, 10, 205–224, doi: 10.1016/0040-1951(70)90107-1.
1653 WESTERCAMP, D. 1979. Diversity, structural control and origin of recent volcanism in the
1654 Lesser Antilles island arc. Bulletin du Bureau de Recherches Géologiques et Minières, Sect.
1655 IV, 211–226.
1656 WESTERCAMP, D. 1988. Magma generation in the Lesser Antilles: geological constraints.
1657 Tectonophysics, 149, 145–163, doi: 10.1016/0040-1951(88)90123-0.
1658 WHITE, N.C. & HEDENQUIST, J.W. 1995. Epithermal gold deposits: styles, characteristics
1659 and exploration. SEG Newsletter, 23, 1–9.
1660 WINCHESTER, J.A. & FLOYD, P.A. 1977. Geochimical discrimination of different magma
1661 series and their differentiation products using immobile elements. Chemical Geology, 20,
1662 325–343, doi: 10.1016/0009-2541(77)90057-2.
1663 YARDLEY, B.W.D. 1989. An Introduction to Metamorphic Petrology. Singapour, Longman
1664 Group UK Ltd.

YARDLEY, B.W.D. 2009. The role of water in the evolution of the continental crust. Journal of the Geological Society, 166, 585–600, doi: 10.1144/0016-76492008-101.

YARDLEY, B.W.D. & CLEVERLEY, J.S. 2015. The role of metamorphic fluids in the formation of ore deposits. Geological Society, London, Special Publications, 393, 117–134, doi: 10.1144/SP393.5.

ZAMI, F., QUIDELLEUR, X., RICCI, J., LEBRUN, J.-F., & SAMPER, A. 2014. Initial sub-aerial volcanic activity along the central Lesser Antilles inner arc: New K–Ar ages from Les Saintes volcanoes. Journal of Volcanology and Geothermal Research, 287, 12–21, doi: 10.1016/j.jvolgeores.2014.09.011.

ZHOU, L., ZHANG, Z., LI, Y., YOU, F., WU, C., & ZHENG, C. 2013. Geological and geochemical characteristics in the paleo-weathering crust sedimentary type REE deposits, western Guizhou, China. Journal of Asian Earth Sciences, 73, 184–198, doi: 10.1016/j.jseaes.2013.04.011.